

Can a regional-scale reduction of atmospheric CO₂ during the COVID-19 pandemic be detected from space? A case study for East China using satellite XCO₂ retrievals

Michael Buchwitz¹, Maximilian Reuter¹, Stefan Noël¹, Klaus Bramstedt¹, Oliver Schneising¹, Michael Hilker¹, Blanca Fuentes Andrade¹, Heinrich Bovensmann¹, John P. Burrows¹, Antonio Di Noia^{2,3}, Hartmut Boesch^{2,3}, Lianghai Wu⁴, Jochen Landgraf⁴, Ilse Aben⁴, Christian Retscher⁵, Christopher W. O'Dell⁶, David Crisp⁷

¹Institute of Environmental Physics (IUP), University of Bremen, 28334 Bremen, Germany

²Earth Observation Science, University of Leicester, LE1 7RH, Leicester, UK

³NERC National Centre for Earth Observation, LE1 7RH, Leicester, UK

⁴SRON Netherlands Institute for Space Research, 3584 CA Utrecht, The Netherlands

⁵Directorate of Earth Observation Programmes, European Space Agency (ESA), ESRIN, 00044 Frascati, Italy

⁶Cooperative Institute for Research in the Atmosphere, Colorado State University (CSU), Fort Collins, CO 80523, USA

⁷Jet Propulsion Laboratory (JPL), Pasadena, CA 91109, USA

Correspondence to: Michael Buchwitz (buchwitz@uni-bremen.de)

Abstract. The COVID-19 pandemic resulted in reduced anthropogenic carbon dioxide (CO₂) emissions during 2020 in large parts of the world. ~~We report results from a first attempt to determine~~[To investigate](#) whether a regional-scale reduction of anthropogenic CO₂ emissions during the COVID-19 pandemic can be detected using space-based observations of atmospheric CO₂. ~~For this purpose,~~ we have analysed a small ensemble of [OCO-2 and GOSAT](#) satellite retrievals of column-averaged dry-air mole fractions of CO₂, i.e. XCO₂. We focus on East China ~~because COVID-19 related CO₂ emission reductions are expected to be largest there early in the pandemic.~~ We analysed four XCO₂ data products from the satellites Orbiting Carbon Observatory 2 (OCO-2) and Greenhouse gases Observing SATellite (GOSAT). We use a data-driven approach that does not rely on *a priori* information about CO₂ sources and sinks and ignores atmospheric transport. Our approach utilises the computation of XCO₂ anomalies, ΔXCO_2 , from the satellite Level 2 data products using a method called DAM (Daily Anomalies via (latitude-band) Medians). DAM removes large-scale, daily XCO₂ background variations, yielding XCO₂ anomalies that correlate with the location of major CO₂ source regions such as East China. We analysed satellite data between January 2015 and May 2020 and compared monthly XCO₂ anomalies in 2020 with corresponding monthly XCO₂ anomalies of previous years. In order to link the XCO₂ anomalies to East China fossil fuel (FF) emissions, we used XCO₂ and corresponding FF emissions from NOAA's (National Oceanic and Atmospheric Administration) CarbonTracker version

CT2019 from 2015 to 2018. Using this CT2019 data set, we found that the relationship between target region ΔXCO_2 and the FF emissions of the target region is approximately linear and we quantified slope and offset via a linear fit. We use the empirically obtained linear equation to compute ΔXCO_2^{FF} , an estimate of the target region FF emissions, from the satellite-derived XCO_2 anomalies, ΔXCO_2 . We focus on October to May periods to minimize contributions from biospheric carbon fluxes and quantified the error of our FF estimation method for this period by applying it to CT2019. We found that the difference of the retrieved FF emissions and the CT2019 FF emissions in terms of the root mean square error (RMSE) is 0.39 GtCO₂/year (4%). We applied our method to NASA's (National Aeronautics and Space Administration) OCO-2 XCO_2 data product (version 10r) and to three GOSAT products. We focus on estimates of the relative change of East China monthly emissions in 2020 relative to previous months. Our results show considerable month-to-month variability (especially for the GOSAT products) and significant differences across the ensemble of satellite data products analysed. The ensemble mean indicates emission reductions by approximately $8\% \pm 10\%$ in March 2020 and $10\% \pm 10\%$ in April 2020 (uncertainties are 1-sigma) and somewhat lower reductions for the other months in 2020. Using only the OCO-2 data product, we obtain smaller reductions of 1-2% (depending on month) with an uncertainty of $\pm 2\%$. The large uncertainty and the differences of the results obtained for the individual ensemble members and use a simple data-driven analysis method. We present estimates of the relative change of East China monthly emissions in 2020 relative to previous periods limiting the analysis to October to May periods to minimize the impact of biogenic CO₂ fluxes. The ensemble mean indicates an emission reduction by approximately $10\% \pm 10\%$ in March and April 2020. However, our results show considerable month-to-month variability and significant differences across the ensemble of satellite data products analysed. For example, OCO-2 suggests a much smaller reduction ($\sim 1-2\% \pm 2\%$). This indicates that it is challenging to reliably detect and to accurately quantify the emission reduction with current satellite data sets. There are several reasons for this including the sparseness of the satellite data but also the weak signal (the expected regional XCO_2 reduction is only on the order of 0.1-0.2 ppm), the sparseness of the satellite data, remaining biases and limitations of our relatively simple data-driven analysis approach. Inferring COVID-19 related information on regional-scale CO₂ emissions using current satellite XCO_2 retrievals likely requires, if at all possible, a more sophisticated analysis method including detailed transport modelling and considering *a priori* information on anthropogenic and natural CO₂ surface fluxes.

1 Introduction

Carbon dioxide (CO₂) is the most important anthropogenic greenhouse gas significantly contributing to global warming (IPCC, 2013). CO₂ has many natural and anthropogenic sources and sinks and our current understanding of them has significant gaps (e.g., Ciais et al., 2014; Chevallier et al., 2014; Reuter et al., 2017c; Crisp et al., 2018; Friedlingstein et al., 2019). Efforts are ongoing to improve the fundamental understanding of the global carbon cycle, to improve our ability to project future changes, and to verify the effectiveness of policies such as the Paris Agreement (<https://unfccc.int/process-and-meetings/the-paris->

Formatiert: Abstand Nach: 0 Pt.

[agreement/the-paris-agreement](#), last access: 8-Sept-2020) aiming to reduce greenhouse gas emissions (e.g., Ciais et al., 2014, 2015; Pinty et al., 2017, 2019; Crisp et al., 2018; Matsunaga and Maksyutov, 2018; Janssens-Maenhout et al., 2020).

Retrievals of XCO₂ from the satellite sensors SCIAMACHY/ENVISAT (Burrows et al., 1995; Bovensmann et al., 1999; Reuter et al., 2010, 2011), TANSO-FTS/GOSAT (Kuze et al., 2016) and from the Orbiting Carbon Observatory-2 (OCO-2) satellite (Crisp et al., 2004; Eldering et al., 2017; O'Dell et al., 2012, 2018) have been used in recent years to obtain information on natural CO₂ sources and sinks (e.g., Basu et al., 2013; Chevallier et al., 2014, 2015; Reuter et al., 2014a, 2017c; Schneising et al., 2014; Houweling et al., 2015; Kaminski et al., 2017; Liu et al., 2017; Eldering et al., 2017; Yin et al., 2018; Palmer et al., 2019; Miller and Michalak, 2020), on anthropogenic CO₂ emissions (e.g., Schneising et al., 2008, 2013; Reuter et al., 2014b, 2019; Nassar et al., 2017; Schwandner et al., 2017; Matsunaga and Maksyutov, 2018; Miller et al., 2019; Labzovskii et al., 2019; Wu et al., 2020; Zheng et al., 2020a; Ye et al., 2020) and for other applications such as climate model assessments (e.g., Lauer et al., 2017; Gier et al., 2020) or data assimilation (e.g., Massart et al., 2016).

Here we use an ensemble of satellite retrievals of XCO₂ to determine whether COVID-19 related regional-scale ([here ~2000² km²](#)) CO₂ emission reductions can be detected and quantified using the current space-based observing system. This is important in order to establish the capabilities of current satellites, which have been optimized to obtain information on natural carbon sources and sinks, but not to obtain information on anthropogenic emissions. Nevertheless, data from existing satellites have already been used to assess anthropogenic emissions (see publications cited above). These assessments and the assessment presented in this publication are relevant for future satellites focussing on anthropogenic emissions such as the planned European Copernicus Anthropogenic CO₂ Monitoring (CO2M) mission (e.g., ESA, 2019; Kuhlmann et al., 2019; Janssens-Maenhout et al., 2020), which is based on the CarbonSat concept (Bovensmann et al., 2010; Velazco et al., 2011; Buchwitz et al., 2013; Pillai et al., 2016; Broquet et al., 2018; [Lespinas et al., 2020](#)).

We focus on China because regional-scale COVID-19 related CO₂ emission reductions are expected to be largest there early in the pandemic (Le Quéré et al., 2020; Liu et al., 2020). Satellite data have been used to estimate China's CO₂ emissions during the COVID-19 pandemic ([as shown in Zheng et al., 2020b](#)), but that study inferred CO₂ reductions from retrievals of nitrogen dioxide (NO₂) not using XCO₂. Estimates of emission reductions have also been derived from bottom-up statistical assessments of fossil fuel use and other economic indicators. According to Le Quéré et al., 2020, China's CO₂ emissions decreased by 242 MtCO₂ (uncertainty range 108 – 394 MtCO₂) during January – April 2020. As China's annual CO₂ emissions are approximately 10 GtCO₂/year (Friedlingstein et al., 2019), i.e., approximately 3.3 GtCO₂ in a 4-month period assuming constant emissions, the average relative (COVID-19 related) change during January – April 2020 is therefore approximately 7% ± 4% (0.242/3.3 ± 0.14/3.3). This agrees reasonably well with the estimate reported in Liu et al., (2020), which is 109.3% for China during the first quarter of 2020 compared to the same period in 2019. Liu et al., (2020) also indicate some challenges in terms of interpreting CO₂ emission reductions as being caused by COVID-19, e.g., the fact that the first months of 2020 were exceptionally warm across much of the northern hemisphere. CO₂ emissions associated with home heating may have

therefore been somewhat lower than for the same period in 2019, even without the disruption in economic activities and energy production caused by COVID-19 and related lockdowns.

Sussmann and Rettinger, 2020, studied ground-based remote sensing XCO₂ retrievals of the Total Carbon Column Observing Network (TCCON) to find out whether related atmospheric concentration changes may be detected by the TCCON and brought into agreement with bottom-up emission reduction estimates. To the best of our knowledge, our study is the first attempt to determine quantitatively. Our study is one of the first attempts to determine whether COVID-19 related regional-scale CO₂ emission reductions can be detected using existing space-based observations of XCO₂, although some qualitative results related to this application are also provided in the internet (e.g., ESA-NASA-JAXA, 2020). Tohjima et al., 2020, inferred estimates of China's CO₂ emissions from modelled and observed ratios of CO₂ and methane (CH₄) surface concentrations at Hateruma Island, Japan. They report for China fossil fuel emission reductions of $32 \pm 12\%$ and $19 \pm 15\%$ for February and March 2020, respectively, which is about 10% higher compared to the results shown in Le Quére et al., 2020 (see Tab.1 of Tohjima et al., 2020). From model sensitivity simulations they conclude that even a 30% reduction of China's fossil fuel CO₂ emissions would only result in a 0.8 ppm XCO₂ reduction over China and that it therefore would be very challenging to detect any COVID-19 related signal with the existing remote sensing satellites GOSAT and OCO-2. Their conjecture has essentially been confirmed by Chevallier et al., 2020. They used XCO₂ from OCO-2 in combination with other data sets and the modelling of CO₂ emission plumes of localized CO₂ sources to obtain estimates of CO₂ emissions focussing on several COVID-19 relevant regions such as China, Europe, India and the USA. They concluded that these places have not been well observed by the OCO-2 satellite because of frequent or persistent cloud conditions and they give recommendations for future carbon-monitoring systems. Zeng et al., 2020, used modelling, GOSAT XCO₂ and other data sets. They conclude that GOSAT is able to detect a short-term global mean XCO₂ anomaly decrease of 0.2-0.3 ppm after temporal averaging (e.g., monthly) but for East China they could not identify a statistically robust COVID-19 related anomaly. Satellite-derived results related to this application are also provided in the internet (e.g., ESA-NASA-JAXA, 2020). Ground-based XCO₂ retrievals of the Total Carbon Column Observing Network (TCCON) have also been used to address this issue (Sussmann and Rettinger, 2020). Sussmann and Rettinger, 2020, studied XCO₂ retrievals to find out whether related atmospheric concentration changes can be detected by the TCCON.

Regional-scale reductions of tropospheric NO₂ columns have been reported for China (e.g., Zhang et al., 2020; Bauwens et al., 2020), but for CO₂ such an assessment is more challenging because of small XCO₂ changes on top of a large background. For example, over extended anthropogenic source areas such as East China, the XCO₂ enhancement due to anthropogenic emissions is typically only approximately 1 - 2 ppm (0.25% - 0.5% of 400 ppm) or even less (see, e.g., Schneising et al., 2008, 2013; Hakkarainen et al., 2016, 2019; Chevallier et al., 2020; Tohjima et al., 2020; and this study). A 10% emission reduction would therefore only change the regional XCO₂ enhancement by 0.1 to 0.2 ppm. This is below the single measurement precision of current satellite XCO₂ data products, (at footprint size, i.e., 10.5 km diameter for GOSAT (Kuze et al., 2016) and 1.3 x 2.3 km² for OCO-2 (O'Dell et al., 2018)), which is about 1.8 ppm (1-sigma) (e.g., Dils et al., 2014;

Kulawik et al., 2016; Buchwitz et al., 2015, 2017a; Reuter et al., 2020) for GOSAT and around 1 ppm for OCO-2 (Wunch et al., 2017; Reuter et al., 2019). ~~This implies that the satellite data need to be averaged to reduce random error (noise) contributions. Therefore, we focus on XCO₂ monthly averages. In our study we focus on XCO₂ monthly averages. Averaging reduces the noise of the satellite retrievals (e.g., Kulawik et al., 2016) but also eliminates day-to-day XCO₂ variations (e.g., Agustí-Panareda et al., 2019), which cannot be interpreted using our simple analysis methods.~~ The accuracy of the East China satellite XCO₂ retrievals averaged over monthly timescales is difficult to assess because of limited reference data. The validation of the satellite data products is primarily based on comparisons with ground-based XCO₂ retrievals from the TCCON, a relatively sparse network with an uncertainty of about 0.4 ppm (Wunch et al., 2010). ~~The estimated precision and accuracy of the satellite XCO₂ retrievals as obtained from comparisons with TCCON XCO₂ retrievals is typically on the order of 0.7 ppm (e.g., Buchwitz et al., 2017a; Reuter et al., 2020) but this estimate assumes error-free TCCON retrievals, i.e., it neglects the non-negligible uncertainty of TCCON.~~

~~The purpose of this study is to investigate - using satellite XCO₂ retrievals - if satellite-derived East China fossil fuel (FF) CO₂ emissions in 2020 (COVID-19 period) differ significantly compared to pre-COVID-19 periods. Ideally, we would like to know by how much emissions have been reduced due to COVID-19. This question, however, cannot be answered using only satellite data because they do not contain any information on how much would have been emitted without COVID-19. Instead, we aim at answering the following question: Are satellite-derived East China FF CO₂ emissions early in the pandemic (here: January – May 2020) significantly lower compared to pre-COVID-19 periods?~~

~~To answer this question, we analyse relative differences of estimates of East China monthly FF emissions during different time periods. We focus on October to May periods and we refer to different periods via the year where a period ends, i.e., we call the period October 2019 to May 2020 “year 2020 period” or simply “2020”, the period October 2018 to May 2019 is called 2019, etc. Specifically, we compute and analyse differences of monthly emissions in the year 2020 period relative to previous year 2016 to 2019 periods, i.e., we use 4 periods for comparison with the year 2020 period. To focus on the COVID-19 aspect, we subtract for each period the October to December (OND) mean value and we refer to these time series as OND anomalies. These OND anomalies are time series at monthly resolution of relative emission difference between different periods relative to OND. Negative OND anomalies during the COVID-19 period would then suggest (depending on uncertainty) that an emission reduction during the COVID-19 period has been detected.~~

~~The structure of our manuscript is structured as follows reflects this procedure: In Sect. the Data Section 2 we present the satellite and model input data used for this study and in Sect., In the Methods Section 3 we present the analysis method. The, which consists of two main section is Sect. 4 where steps. The purpose of the first step is to isolate the East China FF emission signal from the XCO₂ satellite retrievals. This is done by subtracting appropriate XCO₂ background values from the XCO₂ retrievals to obtain XCO₂ anomalies, ΔXCO_2 . We use two methods to compute ΔXCO_2 . We describe one method, the “DAM method”, in detail in Sect. 3.1 and only shortly explain the second method (“TmS method”) referring for details to Appendix A. In the second step (Sect. 3.2) we compute estimates of East China monthly FF CO₂ emissions from the XCO₂~~

anomalies. These emission estimates are then used to compute the OND anomalies explained above. In Results Section 4 we present and discuss the results, i.e., the application of the described methods to the satellite data. A summary and conclusions are given in Sect. 5.

2 Data

In this section, we present a short overview about the input data used for this study.

2.1 Satellite XCO₂ estimates retrievals

This study uses four satellite XCO₂ Level 2 (L2) data products. An overview about these data sets is provided in Tab. 1 including references and access information. The first product listed in Tab. 1 is the latest version of the bias-corrected OCO-2 XCO₂ product delivered to the Goddard Earth Science Data and Information Services Center (GES DISC) by the OCO-2 team (ACOS v10r Lite). The other three satellite XCO₂ datasets are different versions of the GOSAT XCO₂ product derived using retrieval algorithms developed by groups at the University of Leicester, U.K. (UoL-FP v7.3), the SRON Netherlands Institute for Space Research (RemoTeC v2.3.8), and the University of Bremen, Germany (FOCAL v1.0).

The XCO₂ estimates derived from OCO-2 (e.g., O'Dell et al., 2018) and GOSAT (e.g., Kuze et al., 2016) observations are complementary because these two spacecraft use different sampling strategies. OCO-2 has been operating since September 2014. Its spectrometers collect about 85000 cloud-free XCO₂ soundings each day along a narrow (< 10 km) ground track as it orbits the Earth 14.5 times each day from its sun synchronous 1:36 PM orbit. The OCO-2 soundings provide continuous measurements with relatively high spatial resolution ($1.3 \times 2.25 \text{ km}^2$) along each track, but the individual ground tracks are separated by almost 25° longitude in any given day. This spacing is reduced to approximately 1.5° longitude after a 16-day ground track repeat cycle. GOSAT has been returning 300 to 1000 cloud-free XCO₂ soundings each day since April 2009. Its TANSO-FTS spectrometer collects soundings with ~10.65 km diameter surface footprints, separated by approximately 250 km along and across its ground track as it orbits from north to south across the sunlit hemisphere.

2.2 Model CO₂ data

We use data from NOAA's (National Oceanic and Atmospheric Administration) CO₂ assimilation system, CarbonTracker (CT2019) (Jacobson et al., 2020; Peters et al., 2007) to define the relationship between XCO₂ anomalies and fossil fuel emissions. CarbonTracker is a global atmospheric inverse model that assimilates atmospheric CO₂ measurements as well as estimates of emissions from fossil fuels and fires and other sources into an atmospheric transport model to estimate emissions and uptake of CO₂ by the land biosphere and oceans. An overview about CT2019 set is provided in Tab. 2 including references and access information. A description of CT2019 can also be found on the CT2019 website (<https://www.esrl.noaa.gov/gmd/ccgg/carbontracker/index.php>, last access: 24 September 2020): "CarbonTracker produces model predictions of atmospheric CO₂ mole fractions, to be compared with the observed atmospheric CO₂ mole fractions. The

Formatiert: Abstand Nach: 0 Pt., Zeilenabstand: einfach

195 difference between them is attributed to differences in the sources and sinks used to make the prediction (the so-called 'first-guess') and the sources and sinks affecting the true atmospheric CO₂. Using numerical techniques, these differences are used to solve for a set of sources and sinks that most closely matches the observed CO₂ in the atmosphere. to produce modelled fields of atmospheric CO₂ mole fractions by adjusting land biosphere and ocean CO₂ surface fluxes. An overview about CT2019 set is provided in Tab. 2 including references and access information. In short, CarbonTracker has a representation of atmospheric transport based on weather forecasts, and modules representing air-sea exchange of CO₂, photosynthesis and respiration by the terrestrial biosphere, and release of CO₂ to the atmosphere by fires and combustion of fossil fuels."

Formatiert: Absatz-Standardschriftart

Formatiert: Absatz-Standardschriftart

3. Methods

To analyse the satellite data with respect **3.1 Methods to regionally elevated compute XCO₂ due to anomalies (ΔXCO₂)**

205 Satellite XCO₂ retrievals contain information on anthropogenic CO₂ emissions, we (e.g., Schneising et al., 2013; Reuter et al., 2014b, 2019; Nassar et al., 2017) but extracting this information requires appropriate data processing and analysis. For a strong (net) source region XCO₂ is typically higher compared to its surrounding area. Our method is based on computing and subtracting XCO₂ background values. The purpose of this background correction is to isolate the regional emission signal by removing large-scale spatial and day-to-day temporal XCO₂ variations, which cannot be dealt with in our simple data-driven method to estimate emissions.

210 XCO₂ varies temporally and spatially (e.g., Agustí-Panareda et al., 2019; Reuter et al., 2020; Gier et al., 2020), for example, due to quasi-regular uptake and release of CO₂ by the terrestrial biosphere, which results in a strong seasonal cycle, especially over northern mid and high latitudes. Compared to fluctuations originating from the interaction of the terrestrial biosphere and the atmosphere, the spatio-temporal XCO₂ variations due to anthropogenic fossil fuel (FF) CO₂ emissions are typically much smaller (e.g., 1 ppm compared to 10 ppm (Schneising et al., 2008, 2013, 2014; Agustí-Panareda et al., 2019)).

215 A method used for background correction is the one described in Hakkarainen et al., 2019 (see also Hakkarainen et al., 2016, for a first publication of that method). We use a method referred to two different methods for background correction. We refer to these methods as DAM ("Daily Anomalies via (latitude band) Medians), The-" (DAM-method), which is essentially identical with the method described in Hakkarainen et al., 2016 and 2019. They 2019, and a second method called "Target minus Surrounding" (TmS).

220 Hakkarainen et al., 2019, applied their method to the OCO-2 Level 2 XCO₂ data product to filter out trends and seasonal variations in order to isolate CO₂ source/sink signals. For background correction, Hakkarainen et al., 2019, explain their method as follows: "In order to obtain the background, we calculate the daily medians for each 10-degree latitude bandbands and linearly interpolate the resulting values to each OCO-2 data point. The median was chosen because it better represents

Formatiert: Schriftart: Fett

Formatiert: Schriftart: Fett

Formatiert: Schriftfarbe: Automatisch

the typical value in each latitude band, and it is not skewed towards extreme values”. Our approach is very similar, but instead Instead of interpolation, we compute the median around each latitude (“running median”) using a latitude band width of ± 15 deg. We use a larger width compared to Hakkarainen et al., 2019, because we also apply our method to GOSAT data, which are much sparser than OCO-2 data. Our investigations showed that the width of the latitude band is not critical but, The band needs to be wide enough to contain a statistically significant sample, but narrow enough to resolve large latitudinal gradients in CO₂. We subtract the corresponding median from each single XCO₂ observation as contained in the original Level 2 XCO₂ data product files to obtain a data set of XCO₂ anomalies, ΔXCO_2 . For illustration, we gridded these anomalies to obtain global maps. Figure 1 shows such a DAM XCO₂ anomaly map at $1^\circ \times 1^\circ$ resolution covering the time period 2015–2019. The resulting spatially resolved XCO₂ anomalies are very similar as the one shown in Hakkarainen et al., in the original Level 2 XCO₂ data product files to obtain a data set of XCO₂ anomalies, ΔXCO_2^{DAM} , 2019 (see their Fig. 3, top panel). The good agreement confirms the finding reported above that the generation of these anomaly maps does not critically depend on how exactly the median is computed and used to subtract “the background”.

A zoom into Fig. 1 is presented in Fig. 2, which shows more details for China and surrounding areas. As can be seen from Fig. 2, the DAM ΔXCO_2 has a positive anomaly especially in the region between Beijing, Wuhan and Hong Kong with highest values in the area between Beijing and Shanghai. This positive anomaly indicates that this region is an important CO₂ source region. Of course, there is no one-to-one correspondence (especially not for every grid cell) between these XCO₂ anomalies and local CO₂ emissions (or uptake) because the emitted CO₂ is transported and mixed in the atmosphere. Furthermore, the satellite data are typically sparse due to strict quality filtering to avoid potential XCO₂ biases, for example, due to the presence of clouds. Cloud contaminated ground scenes are identified to the extent possible via the corresponding retrieval algorithm and flagged to be “bad” (see references listed in Tab. 1) and are therefore not used for this analysis. The sparseness of the satellite data set is obvious from Fig. 3, which shows DAM XCO₂ anomaly maps for the month of February during the six years from 2015 to 2020.

The geographical coordinates of the East China target region investigated here are listed in Tab. 3. The fossil fuel (FF) CO₂ emissions of this target region are approximately 8 GtCO₂/year, i.e., the selected target region covers approximately 80% of the FF emissions of entire China, which are approximately 10 GtCO₂/year (Le Quéré et al., 2018; Friedlingstein et al., 2019).

For our East China analysis, we compute regional averages of DAM. In order to verify that our results do not critically depend on the details of one method we also use the second TmS method. Here we obtain the background by averaging XCO₂ in a region surrounding the target region (see Tab. 3 for the latitude and longitude corner coordinates of the target and its surrounding region).

We call these background corrected XCO₂ retrievals XCO₂ anomalies and satellite-derived maps and time series of these XCO₂ anomalies by averaging the ΔXCO_2 values for all satellite ground scenes (footprints) as located in the East China

Formatiert: Schriftfarbe: Automatisch

Formatiert: Schriftfarbe: Automatisch

Formatiert: Schriftfarbe: Automatisch

Formatiert: Zeilenabstand: 1.5 Zeilen

target region for each day in the period January 2015 to May 2020 are presented and discussed in Sect. 4.1. These East China daily time series XCO_2 anomalies are then further averaged used to obtain monthly compute East China ΔXCO_2 CO_2 emission estimates, CO_2^{FF} , as presented described in the following sub-section.

4. Results and discussion

4.1 Application of the DAM method to model data

3.2 Computation of emission estimates (CO_2^{FF})

To determine whether satellite XCO_2 retrievals can provide information on relative changes of anthropogenic CO_2 emissions for the East China target region, we must establish the relationship between the DAM- XCO_2 anomalies (see Sect. 3.1) and the desired estimates of the target region fossil fuel (FF) emissions. For this purpose To develop a method to convert the XCO_2 anomalies, ΔXCO_2 , to FF emission estimates, CO_2^{FF} , we use an existing model data set, the CarbonTracker (CT2019) data set described in Sect. 2.2, which contains atmospheric CO_2 fields and corresponding CO_2 surface fluxes during 2015 – 2018.

Figure 4.1 shows CT2019 XCO_2 maps (left) and corresponding surface CO_2 flux maps (right) for selected days in the January to May 2018 period. The XCO_2 has been computed by vertically integrating the CT2019 CO_2 vertical profiles (weighted with the surface pressure normalized pressure change over each layer). The model data are sampled at local noon, which is close to the overpass time of the satellite data sets used here. The spatio-temporal sampling of a specific satellite XCO_2 data product is not considered here, i.e., we use the CT2019 data set independent of any satellite data product apart for the sampling at local noon. As can be seen from Fig. 1 As can be seen from Fig. 4, XCO_2 is clearly elevated over the East China target region (red rectangle) relative to its surrounding region on 15-January-2018 (panel-Fig. 1(a)) and on 15-March-2018 (panel-Fig. 1(c)). On 15-May-2018 (panel-Fig. 1(e)) the target region and parts of the surrounding region contain large areas of lower than average XCO_2 , a pattern which primarily results from carbon uptake by vegetation during the growing season, which starts in eastern China around May each year. The CO_2 fluxes, which are shown in on the right-hand side panels of Fig. 4.1, show similar spatial pattern as the XCO_2 maps but as already explained, due to atmospheric transport and the long lifetime of atmospheric CO_2 there is not and one-to-one correspondence between atmospheric XCO_2 and surface emissions due to atmospheric transport. The CO_2 fluxes are the sum of several contributing fluxes including FF emissions, biospheric biogenic fluxes and other fluxes (e.g., due to fires and the oceans).

Figure 5.2(a) shows time series obtained by applying the DAM method to CT2019 XCO_2 for the East China target region. The top panel shows The CT2019 data set not only contains atmospheric CO_2 concentrations but also its components due to fossil fuel (FF) emissions and biogenic (BIO) and other fluxes. From the CT2019 FF emissions as thick red line. For each day, data set we computed total XCO_2 (TOT), and its FF and BIO components. From these components we subtracted the background

Formatiert: Schriftfarbe: Automatisch

Formatiert: Schriftfarbe: Automatisch

Formatiert: Schriftfarbe: Automatisch

Formatiert: Schriftfarbe: Automatisch

Formatiert: Schriftfarbe: Automatisch

Formatiert: Schriftfarbe: Automatisch

Formatiert: Schriftfarbe: Automatisch

Formatiert: Schriftart: Nicht Fett

Formatiert: Schriftfarbe: Automatisch

290 using the DAM method and the corresponding monthly $\Delta\text{XCO}_2^{\text{DAM}}$ time series are shown in Fig. 2(a). As can be seen from Fig. 2(a), total $\Delta\text{XCO}_2^{\text{DAM}}$ (black line) is dominated by its FF (red line) and BIO (green line) components (their sum, i.e., FF + BIO (grey line), is close to compute daily (and then monthly) TOT (black line)). As can also be seen, FF emissions for East China (red line) are larger than the BIO fluxes (green line) at least during October to April. During May to September the BIO fluxes are negative due to uptake of atmospheric CO_2 by the terrestrial biosphere and their absolute value is on the same order or may even significantly exceed the FF emissions. As a consequence, total $\Delta\text{XCO}_2^{\text{DAM}}$ (black line) gets negative. During these months, the total anomaly (black line) is closer to BIO (green line) than to FF (red line).

The task for the satellite inversion is to obtain estimates of East China FF CO_2 emissions from the satellite-derived (total) XCO_2 anomalies, ΔXCO_2 . The monthly CT2019 ΔXCO_2 values were linearly fitted to $\Delta\text{XCO}_2^{\text{DAM}}$ (black line in Fig. 2(a)). To determine to what extent this is possible, we fitted to the monthly CT2019 $\Delta\text{XCO}_2^{\text{DAM}}$ (i.e., the quantity that we can also obtain from satellites) to the East China CT2019 FF CO_2 emissions to obtain a quantity referred to as $\Delta\text{XCO}_2^{\text{FF}}$; (which closely resembles the FF known “true emissions as shown” in the top panel of Fig. 5; this model data assessment exercise). The linear fit yields $\Delta\text{XCO}_2^{\text{FF}} = 0.914 \times \Delta\text{XCO}_2 + 7.106$, with ΔXCO_2 in parts per million (ppm) and $\Delta\text{XCO}_2^{\text{FF}}$ in $\text{GtCO}_2/\text{year}$. Using this linear transformation, ΔXCO_2 can be transformed into $\Delta\text{XCO}_2^{\text{FF}}$ and daily and monthly $\Delta\text{XCO}_2^{\text{FF}}$ values results are shown in Fig. 5 as thin grey line and blue dots, respectively; 2(b) for October to May periods. The estimated emissions (black crosses) have been obtained via a linear fit of $\Delta\text{XCO}_2^{\text{DAM}}$ to the CT2019 FF emissions (red dots). The two parameters of the linear fit are also shown in 2(b): Scaling factor A (= 0.90) and offset B (= 7.41). As can be seen, the estimated emissions agree reasonably well with the “true” emissions. The linear correlation coefficient R is 0.83 (see Fig. 2(c)) and the relative difference in terms of mean and standard deviation is $0.2\% \pm 5\%$ (see Fig. 2(d)). However, for individual months the error can be as large as 10%. From this we conclude that the (approximately 2-sigma) uncertainty of our method is approximately 10%.

Initially, we assumed that ΔXCO_2 is a similar figure but generated using the TmS method is shown in Appendix A as Fig. A1. As can be seen, the results shown in Fig. A1 (b) to (d) are similar to the ones shown in Fig. 2 (b) to (d) but the linear correlation is slightly worse and the errors are slightly larger. In contrast, the time series shown in panels (a) differ significantly. This is because of the different background corrections used for the two methods. But despite these significant differences the quality of the derived emissions is similar (the standard deviation of the monthly biases is 5.5% for TmS and 4.8% for DAM, see panels (d)). Nevertheless, the DAM method gives slightly better results compared to the TmS method and this is also confirmed by applying both methods to the satellite data (see Sect. 4). Therefore, the DAM method is our baseline method and we focus on results obtained with the DAM method.

It is perhaps surprising that the offset (fit parameter B, see above) is so large (7.41 for DAM and 7.63 for TmS). Probably one would assume that the XCO_2 anomalies ΔXCO_2 are directly proportional to the target region fossil fuel emissions, i.e., we assumed one would assume that FF is (approximately) equal to a constant multiplied by ΔXCO_2 (no offset added). If we were (for example, for $\text{FF} = 8 \text{ GtCO}_2/\text{year}$ and $\Delta\text{XCO}_2 = 2 \text{ ppm}$ one would have expected that the conversion factor is 4

Formatiert: Schriftfarbe: Text 1

Formatiert: Schriftfarbe: Text 1

Formatiert: Schriftfarbe: Text 1

Formatiert: Schriftfarbe: Text 1

Formatiert: Schriftfarbe: Text 1

Formatiert: Schriftfarbe: Text 1

Formatiert: Schriftfarbe: Text 1

Formatiert: Schriftfarbe: Text 1

Formatiert: Schriftfarbe: Text 1

Formatiert: Schriftfarbe: Text 1

Formatiert: Schriftfarbe: Text 1

GtCO₂/year/ppm). In that case, as we are only interested in relative changes in emissions, we would not need to know the exact value of the scaling factor. However, when analysing the satellite data, we found that ΔXCO_2 is around 2 ppm for January but decreases in subsequent months, nearly approaching zero in May (which is consistent with the CT2019 results shown here but see in Fig. 5, top panel, showing a time series of ΔXCO_2^{FF} (blue dots)). As anthropogenic emissions are not expected to change that much within a few months (and zero emissions around May are not realistic at all) we concluded that the simple proportionality assumption does not hold. To investigate this we used the CT2019 data set to test and improve our method; and the results are reported in this section. We applied our method to CT2019 XCO₂ (as shown in Fig. 2) and compared the retrieved FF values with the (“true”) CT2019 FF values as used by CT2019. We found large differences, which could be significantly reduced by adding an offset. To obtain numerical values for the offset (see parameter B in Fig. 5, top panel) and for the scaling factor (see parameter A in Fig. 5, top panel) we used a linear fit as discussed above. The reason for the large offset is the influence of the biosphere. Around May the uptake of atmospheric CO₂ due to the biosphere is so large that ΔXCO_2 is close to zero - but the FF emissions are not - and the East China target regions is essentially “carbon neutral” or even a net sink (see also Fig. 1).

As explained above, i.e., these two parameters, scaling factor A and offset B are obtained empirically via a linear fit using CT2019 data (Fig. 2(b)) and used for the conversion of the satellite XCO₂ anomalies during the entire time period January 2015 to May 2020 (as will be shown in Sect. 4). As can be seen from Fig. 2 (b) and (c), the retrieval biases are within $\pm 10\%$ during 2015–2018. We assume in our study that the same conversion is also appropriate for 2019 and 2020. However, it cannot be ruled out that 2019 or 2020 were significantly different compared to previous years with respect to aspects relevant for our study. To address this, we compare period October 2019 to May 2020 results with the corresponding results from previous October to December periods to find out to what extent the period of interest, i.e., October 2019 to May 2020, is significantly different taking into account the year-to-year variability, which we use to obtain uncertainty estimates.

We use target region monthly ΔXCO_2^{FF} as a satellite-based estimate of target region monthly FF emissions. The middle and the bottom panels of Fig. 5 show the absolute and the relative monthly differences between ΔXCO_2^{FF} and the FF emissions, respectively. Also listed are several quantities used to characterise the level of agreement/disagreement: D is the mean difference, S is the standard deviation of the difference, RMSE is the root-mean-square error and R is the linear correlation coefficient of the monthly ΔXCO_2^{FF} and FF values. As can be seen, the RMSE is 0.45 GtCO₂/year (6%) for the entire time series 2015–2018. The RMSE is reduced to 0.39 GtCO₂/year (4%) if the analysis is restricted to time periods covered by the months October to May, which is the relevant period for this study as it covers pre-COVID-19 (October–December 2019) and COVID-19 (January–May 2020) periods. Excluding June to September data reduces the RMSE because (during this summer period) disturbances from biospheric fluxes (i.e., photosynthesis related fluxes during the vegetation growing season) are largest. As shown in Fig. 5, ΔXCO_2^{FF} is to a good approximation proportional to FF emissions and for this study it is assumed that relative changes of the monthly ΔXCO_2^{FF} values can be used as a sufficiently accurate proxy for relative changes of the monthly FF emissions.

~~The method~~The methods described in this section ~~has~~have been applied to convert satellite-derived target region XCO₂ anomalies, ΔXCO₂, into ΔXCO₂^{FF}. Monthly ΔXCO₂^{FF} values have been computed for each satellite data product and used to find out if FF reductions during the COVID-19 pandemic can be detected in these time series, as will be estimated target region FF CO₂ emissions, CO₂^{FF}. How this has been done using the DAM method for background correction is explained in the following sub-sections. Sect. 4, where we refer for the corresponding TmS method results to Appendix A.

4. Results and discussion

In this section, we present results obtained by applying the DAM method (see Methods Sect. 3.1) to the satellite data to obtain XCO₂ anomalies from which we derive FF emission estimates (see Methods Sect. 3.2).

4.2.1 Application of the DAM method to satellite XCO₂ retrievals

The DAM method has been applied to the OCO-2 and GOSAT satellite XCO₂ data products listed in Tab. 1. Figure 3 shows a global OCO-2 DAM XCO₂ anomaly map at 1°x1° resolution for the period 2015 – 2019. A similar map is shown in Hakkarainen et al., 2019 (see their Fig. 3, top panel). The degree of agreement confirms the finding reported in Sect. 3.1 that the generation of these anomaly maps does not critically depend on how exactly the median is computed and used to subtract “the background”. Hakkarainen et al., 2019, discuss their OCO-2 derived maps in quite some detail also in terms of seasonal averages and comparisons with model simulations. They show that positive anomalies correspond to fossil fuel combustion over major industrial areas including China. Their seasonal maps (see their Fig. 4) show a strong positive anomaly over East China (similar as shown here in Fig. 3) except for the June-August (JJA) summer season, where the XCO₂ anomaly can be negative. This is consistent with the CT2019 results presented in Sect. 3.2.

A zoom into Fig. 3 is presented in Fig. 4, which shows more details for China and its surrounding area. As can be seen from Fig. 4, ΔXCO₂^{DAM} is positive especially in the region between Beijing, Wuhan and Hong Kong with highest values in the area between Beijing and Shanghai. This positive anomaly indicates that this region is a strong CO₂ source region as also discussed in Hakkarainen et al., 2019. As already explained, there is no one-to-one correspondence (especially not for every grid cell) between local XCO₂ anomalies and local CO₂ emissions (or uptake) because the emitted CO₂ is transported and mixed in the atmosphere. Furthermore, the satellite data are typically sparse due to strict quality filtering to avoid potential XCO₂ biases, for example, due to the presence of clouds. Cloud contaminated ground scenes are identified to the extent possible via the corresponding retrieval algorithm (see references listed in Tab. 1) and flagged to be “bad” and are therefore not used for this analysis. The sparseness of the satellite data set is obvious from Fig. The DAM method described in the previous section has been applied to a small ensemble of XCO₂ retrievals from OCO-2 and GOSAT (see details listed in

Formatiert: Schriftart: Nicht Fett

Formatiert: Schriftfarbe: Text 1

Tab. 1) and the results are presented below. As noted above, a5, which shows OCO-2 DAM XCO₂ anomaly maps for February during the six years 2015 to 2020.

A key difference between the OCO-2 and the GOSAT data products is the different sampling of the target region, with GOSAT having much sparser coverage compared to OCO-2. This is illustrated in Fig. 6, which shows February to March 2020 averages of the OCO-2 XCO₂ data product (Fig. 6a) and the three GOSAT data products (Fig. 6b – 6d) at 1°x1° resolution. The OCO-2 product shown in Fig. 6a is NASA’s OCO-2 operational “Atmospheric CO₂ Observations from Space” (ACOS) algorithm version 10r bias corrected XCO₂ product (the so called Lite product), which is referred to in this publication via the product identifier (ID) CO2_OC2_ACOS. The three GOSAT XCO₂ products are (see details and references as given in Tab. 1): Fig. 6b: University of Leicester’s GOSAT product (ID CO2_GOS_OCFP); Fig. 6c: SRON Netherlands Institute for Space Research GOSAT product (CO2_GOS_SRFP); Fig. 6d: University of Bremen’s GOSAT product (CO2_GOS_FOCA) as retrieved with the “Fast atmOspheric traCe gAs retrievaL” (FOCAL) retrieval algorithm initially developed for OCO-2 (Reuter et al., 2017a, 2017b). As can be seen from Fig. 6, the spatial sampling of the target region is different for each product as only quality-filtered (i.e., “good”) data are shown and the quality filtering is algorithm specific (see references listed in Tab. 1).

Figure 6 also shows as red rectangle the East China target region as defined for this study (the geographical coordinates are listed in Tab. 3). The fossil fuel (FF) CO₂ emissions of this target region are approximately 8 GtCO₂/year, i.e., the selected target region covers approximately 80% of the FF emissions of entire China, which are approximately 10 GtCO₂/year (Le Quéré et al., 2018; Friedlingstein et al., 2019). In the following section we present East China FF emission estimates as derived from the satellite XCO₂ anomalies during and before the COVID-19 period.

4.2. Emission estimates

Carbon dioxide fossil fuel emission estimates, CO₂^{FF}, have been derived from the XCO₂ anomalies, ΔXCO₂, computed for each of the four satellite XCO₂ data products listed in Tab. 1. Application. In this section the emission results are presented and discussed. We focus on results based on ΔXCO₂ derived with the DAM method and refer to Appendix A for results based on the TmS method.

Formatiert: Links

Formatiert: Schriftfarbe: Automatisch

Formatiert: Schriftfarbe: Automatisch

Formatiert: Links, Abstand Nach: 0 Pt., Zeilenabstand: einfach

Formatiert: Schriftart: Nicht Fett

Formatiert: Schriftart: Nicht Fett

4.2.1 Emission estimates from NASA's OCO-2 (version 10r) XCO₂

Figure 7 shows the results obtained by applying the DAM method to product CO2_OC2_ACOS (see Tab. 1) for the East China target region for the period January 2015 to May 2020. The top panel (the TmS version of this figure is shown as Fig. A2 in Appendix A). Figure 7(a) shows the daily DAM XCO₂ anomalies as thin grey line and the corresponding monthly averages as red dots. The amplitude (approximately ± 1 ppm) and time dependence (e.g., there is a minimum in the middle of each year) is similar as expected as can be concluded from a comparison with the corresponding for CT2019 results shown in (Fig. 5 (but note 2(a) black line)). To ensure that Fig. 7 shows ΔXCO_2 whereas Fig. 5 shows ΔXCO_2^{FF} , which differs somewhat in amplitude and offset due to the applied linear transformation as explained in Sect. 4.1). Two there are a sufficiently large number of observations per month, two criteria need to be fulfilled for the monthly data shown in this figure: (i) There must be a minimum number of days per month is (here: 5) and (ii) the minimum number of observations per day is (here: 30, i.e., at least 5 days per month having ≥ 30). The latter criterion is also relevant for each day) at least 30 observations per day in the target region need to be available for a month to be accepted (results for the daily data shown in Fig. 7(a) (grey line). We also used other combinations of these two parameters are presented (as shown below), e.g., Fig. 9).

The middle panel of Fig. 7 shows monthly ΔXCO_2^{FF} for October–May for five different periods: October 2019–May 2020 (red), October 2018–May 2019 (blue) and three corresponding periods in earlier years (see annotation as listed in the figure panel). As can be seen from this panel, the red curve (October 2019–May 2020) shows, apart from March 2020, somewhat lower values in the period February 2020–May 2020 (i.e., during the “COVID-19 period”) compared to January 2020 and earlier months (“pre-COVID-19 period”). However, the time dependence shows significant month-to-month variability. Furthermore, a similar time dependency is also present for October 2015–May 2016 (pink). In comparison to the other periods from earlier years, the (red) October 2019–May 2020 values are mostly close to the maximum (or even exceed) the values of the other curves corresponding to earlier October–May time periods.

The bottom panel of Figure 7 shows the corresponding relative differences, as we are mostly interested in relative (percentage) changes of the target region FF emissions. The blue dots (and connecting lines) show the relative difference between the red dots from in the middle panel (this time series ends in May 2020) and the blue dots shown in the middle panel (this time series ends in May 2019). If for simplicity we refer to time series ending in May as “2020” (red dots in middle panel) and “2019” (blue dots in middle panel), then the blue dots displayed in the bottom panel show “(2020–2019)/2019”, i.e., they are a proxy for the relative change of the target region FF emissions of the corresponding months in 2020 relative to 2019 (for January to May; for October to December the difference corresponds to 2019 relative to 2018). The green dots show the corresponding relative differences for 2020 relative to 2018, the orange dots correspond to the relative differences for 2020 relative to 2017 and the pink dots show the relative differences for 2020 relative to 2016. As can be seen from the bottom panel of Fig. 7, the relative difference between the time series ending in May 2020 and in May 2019 (blue dots in the bottom panel) also shows significant variability from month to month. Compared to all previous differences (2020–2018, 2020–2017, etc.) one sees that

these differences are mostly positive and typically somewhere in the range between 0% and +10%. Figure 7 indicates that during October 2019 to May 2020 target region FF emissions are on average a few percent higher compared to previous years.

The data shown in the bottom panel of Fig. 7 are also shown in Fig. 8 (see thin lines using different colours) but together with derived monthly median (and mean) values. In addition, vertical bars are shown to indicate the scatter of the monthly values. As we are primarily interested in changes during the January to May 2020 period compared to preceding months (October–December 2019) and compared to previous years, the median has been computed for each month and the October–December 2019 (i.e., pre-COVID-19 OND months) mean value has been subtracted to highlight the difference of 2020 relative to Figure 7(b) shows monthly ΔXCO_2^{DAM} for different October to May periods and Fig. 7(c) shows the corresponding estimated FF emissions, $CO_2^{FF(DAM)}$. Figure 7(d) shows relative differences of the time series shown in Fig. 7(c). For example, the blue data are referred to as “(2020-2019)/2019” in Fig. 7(d), where 2019 refers to the blue data in Fig. 7(c), which corresponds to the period ending in May 2019. Shown are differences of year 2020 data (red in Fig. 7(c)) minus data from previous periods, i.e., Fig. 7(d) shows to what extent 2020 (strictly speaking the period 10.2019 – 5.2020, i.e., the period which ends in 2020) differs relative to previous October to May periods.

To find out if we can detect a difference between the COVID-19 period and pre-COVID-19 periods, we subtract from each time series shown in Fig. 7(d) the October to December (OND) mean value. The corresponding time series are shown in Fig. 7(e) and are referred to as “OND anomalies” in the following. As can be seen from Fig. 7(e), the OND anomalies vary within $\pm 5\%$. Values before January scatter around zero as the mean value of OND anomalies is zero by definition during October to December. In January the values also scatter around zero. After January most values are negative indicating reduced emissions compared to pre-COVID-19 periods. This can be seen more clearly in Fig. 8, where the same data as in Fig. 7(e) are shown but in addition the ensemble mean (light blue thick lines and dots) and median (royal blue thick lines and dots) has been added including uncertainty estimates as computed from the standard deviation of the ensemble members.

~~2019.~~ The corresponding monthly medians are shown as thick royal blue symbols (and connecting lines) and the scatter—as computed from the standard deviation of the monthly values—is shown as royal blue vertical bars. The light blue symbols and lines show the corresponding values when using the mean instead of the median. In grey, the “original” median values are shown, i.e., in grey, the median values are shown before the offset has been subtracted (i.e., the “absolute” values are shown in grey and the corresponding “OND anomaly” is shown in royal blue). The royal blue curve indicates that ΔXCO_2^{FF} , our proxy for the target region FF emissions, is 2–3% lower in February to April 2020 compared to October to December 2019 and earlier years. Due to the large scatter and significant month-to-month variability and possibly also for other reasons (e.g., the unusual meteorological conditions in the first few months of 2020, see, for example, Liu et al., 2020) it is unclear to what extent this reduction is related to COVID-19 countermeasures.

Formatiert: Schriftfarbe: Text 1

Figures 7 and 8 have been generated with the requirement that, for each day, at least 30 observations need to be available in the target region and ~~that~~ for each month, at least 5 days fulfilling this 30 observations/day requirement ~~are available~~. Figure 9 is similar to Fig. 8 except that ~~also~~ results for additional combinations ~~have been added, i.e., other combinations~~ of minimum number of observations per day and minimum number of days per month ~~have been added. Here, As can be seen~~, the results depend somewhat on which combination of these parameters is used, but the ~~overall end result as shown via the royal blue symbols and lines is fairly stable as it depends only marginally on which set of combinations is used as can be seen when comparing Fig. 9~~ ensemble median and its uncertainty (royal blue symbols and lines) is similar. The ensemble median values ~~are similar and negative during February to May 2020. The large uncertainties (vertical lines; 1-sigma error estimates) reflect the scatter of the ensemble members. The errors bars (1-sigma) overlap with the zero (i.e., no reduction) line indicating that it cannot be claimed with Fig. 8 confidence that a significant drop of the emissions during the COVID-19 period has been detected.~~

4.2.2 Application to Emission estimates from GOSAT XCO₂ data products

The same analysis method as applied to NASA's OCO-2 data product (see Sect. 4.2.1) has also been applied to the three GOSAT XCO₂ data products listed in Tab. 1. The results are shown in Fig. 10 for product CO2_GOS_OCFP, in Fig. 11 for product CO2_GOS_SRFP, and in Fig. 12 for product CO2_GOS_FOCA. ~~The month-to-month variations are larger for these GOSAT products compared to OCO-2 product (note the different scale of the y-axes compared to Fig. 9). This is because GOSAT products are much sparser compared to the OCO-2 product (as shown in Fig. 6) and because the single observation random error is larger for GOSAT compared to OCO-2. As can be seen from a comparison of the results obtained for the three GOSAT products (Figs. 10 - 12) there are large difference among the results obtained from these products. For example, product CO2_GOS_OCFP (Fig. 10) suggests that the largest emission reduction is in April, in contrast to the other two products. The large spread of the GOSAT results means that no clear conclusions can be drawn concerning East China emission reductions during the COVID-19 period.~~

~~The month-to-month variations are larger for these products compared to product CO2_OC2_ACOS (e.g., Figs. 9; note the different scales of the y-axes). This is very likely because GOSAT products are sparse compared to the OCO-2 product (see Fig. 6) but also because the single observation random error (precision) is larger for GOSAT.~~

~~Analysis of product CO2_GOS_OCFP (Fig. 10) suggests that on average, emissions are reduced in 2020 (approximately 12% ± 12%) but strong conclusions cannot be drawn because of large uncertainty (approximately 12%, 1-sigma). Product CO2_GOS_SRFP (Fig. 11) shows no clear time dependence due to large month-to-month variability and the same seems to be true for product CO2_GOS_FOCA (Fig. 12).~~

4.2.3 Ensemble mean and uncertainty

An overview about the results obtained from all four satellite data products [using the DAM method](#) is shown in Fig. 13. ~~(the corresponding TmS version of this figure is shown as Fig. A3 in Appendix A).~~ The results obtained from the individual products (as shown in royal blue in Figs. 9 - 12) are shown here using reddish colours (the corresponding numerical values are listed in Tab. 4). Also shown in Fig. 13 is the mean of the ensemble members and its estimated uncertainty (in dark blue); the corresponding numerical values are listed in the bottom row of Tab. 4. ~~In Fig. 13, the~~ ensemble mean ~~shows on average slightly lower values during March and April 2020 compared to the other months, suggesting an emission reduction suggests emission reductions by several percent~~ ($\approx 10\% \pm 10\%$ in March and $\approx 10\%$ in April), 2020. However, the 1-sigma uncertainties shown as dark blue vertical lines are large ($\pm 10\%$) and typically overlap with the zero, i.e., no change, line. Furthermore, as already discussed can also be seen, there are considerable month-to-month variations and significant differences across the ensemble of satellite data products. For example, the analysis of the OCO-2 data suggests a much smaller emission reduction of only about 1-2%. Because of the large differences between the results obtained from the individual satellite data products, ~~its ensemble members it is therefore~~ concluded that the expected [emission](#) reduction cannot be [reliably detected and accurately quantified with our method](#).

5 Summary and conclusions

We have analysed a small ensemble of ~~retrieved~~ satellite XCO₂ data products to investigate whether a regional-scale reduction of atmospheric CO₂ during the COVID-19 pandemic can be detected ~~everfor~~ East China. Specifically, we analysed four XCO₂ data products from the satellites OCO-2 and GOSAT. For this purpose, we used a [simple](#) data-driven approach, which involves the computation of XCO₂ anomalies, ΔXCO_2 , using a method called DAM (Daily Anomalies via (latitude band) Medians). This method, which is essentially identical with the method developed at Finnish Meteorological Institute (FMI, Hakkarainen et al., 2019), helps to isolate local or regional XCO₂ enhancements originating from anthropogenic CO₂ emissions from large-scale daily XCO₂ background variations: [\(note however that the FMI method is not supposed to extract exclusively anthropogenic emission contributions to XCO₂, see Hakkarainen et al., 2019\).](#) In addition to the DAM method we also used a second method for the computation of ΔXCO_2 , which is referred to TmS (Target minus Surrounding). Using model and satellite data we found that the results obtained with the DAM method provide better results compared to the TmS method. Therefore, [we focussed on DAM-based results but also report selected results obtained with the TmS method \(reported separately in Appendix A\).](#) We analysed satellite data between January 2015 to May 2020 and compared year 2020 monthly XCO₂ anomalies with the corresponding monthly XCO₂ anomalies from previous ~~months~~ periods.

In order to link the satellite-derived XCO₂ anomalies to East China fossil fuel (FF) CO₂ emissions, we used output from NOAA's CO₂ assimilation system CarbonTracker (CT2019-), [covering the years 2015 to 2018. We focus on October to May](#)

Formatiert: Zeilenabstand: 1.5 Zeilen

Formatiert: Zeilenabstand: 1.5 Zeilen

periods to minimize the impact of the terrestrial biosphere. Using CT2019, we show that ΔXCO_2 can be linearly transformed/converted to “FF related XCO_2 -enhancements”-emission estimates, denoted $\Delta XCO_2^{FF}, CO_2^{FF}$, via a linear transformation. The two coefficients slope and offset of this linear transformation have been obtained empirically via a linear fit, i.e., we established a linear empirical equation to relate these two quantities. We use this empirical equation to compute ΔXCO_2^{FF} , an estimate of the target region FF emissions, from the satellite-derived XCO_2 -anomalies, ΔXCO_2 . We focus on October to May periods and found CO_2^{FF} . We show using CT2019 that the root-mean-square-error (RMSE) of retrieved emissions during October to May periods agree within 10% with the CT2019 East China FF emissions.

For the analysis of the satellite data we focus on the October 2019 to May 2020 period, which covers months during the COVID-19 pandemic but also pre-COVID-19 months. We compare results obtained during this period with earlier October to May periods to find out to what extent year 2020 differs from previous years. Our analysis is limited to October to May periods because our FF-estimations simple data-driven analysis method is approximately 0.39 GtCO₂/year (4%). These months are less affected by disturbances from natural terrestrial vegetation carbon cannot deal with the large and highly variable terrestrial biosphere CO₂ fluxes (using all months the RMSE outside of this period. On the other hand this period is larger, namely 0.45 GtCO₂/year or 6%) and appropriate as they cover relevant pre-COVID-19 (e.g., October–December 2019) and COVID-19 (January–May 2020) periods. However, challenging for satellite retrievals during these months are more challenging because of the low sun angles especially during the winter months and cloudiness.

We applied our method to each of the four satellite XCO₂ data products and computed to obtain monthly ΔXCO_2^{FF} emission estimates, CO_2^{FF} , for East China (“retrieved East China monthly FF emissions”). We focus on changes relative to pre-COVID-19 periods. Our results show considerable month-to-month variability (especially for the GOSAT products) and significant differences across the ensemble of satellite data products analysed. The ensemble mean suggests emission reductions by approximately $8\% \pm 10\% \pm 10\%$ in March 2020 and $10\% \pm 10\%$ in April 2020 (uncertainties are 1-sigma) and somewhat lower reductions for the other months in 2020. These values are. This estimate is dominated by the GOSAT ensemble members. Analysis of the OCO-2 product yields smaller values showing indicating a reduction of only about 1-2% with an uncertainty of approximately $\pm 2\%$.

The large uncertainty, which is on the order of the derived reduction (i.e., 100%, 1-sigma), and the large spread of the results obtained for the individual ensemble members, indicates that it is challenging to reliably detect and to accurately quantify the emission reduction using the current generation of space based methods and the simple DAM-based analysis strategy adopted here.

These findings, which are consistent with other recent studies (e.g., Chevallier et al., 2020, Zeng et al., 2020), are not unexpected. Fossil fuel emissions related regional XCO₂ enhancements due to fossil fuel emissions are typically only 1 to 2 ppm and even a 10% emission reduction would therefore only correspond to a reduction of the fossil fuel related regional XCO₂ enhancement by 0.1 to 0.2 ppm. XCO₂ variations as small as 0.2 ppm are below the estimated uncertainty of the single

footprint satellite XCO₂ retrievals. ~~This~~The uncertainty of single observations ~~uncertainty~~, which is typically around 0.7 ppm (e.g., Buchwitz et al., 2017a; Reuter et al., 2020), has been obtained by comparisons with ground-based Total Carbon Column Observing Network (TCCON) XCO₂ retrievals, which have an uncertainty of 0.4 ppm (1-sigma, Wunch et al., 2010). ~~To reduce random errors,~~In this study we usefocus on monthly averaged data because our analysis method cannot properly deal with day-to-day variability and because of the sparseness of the satellite data. Averaging results in reducing the random error but investigations have shown that random errors do not simply scale with the inverse of the square root of number of observations added (Kulawik et al., 2016). ~~due to (unknown) systematic errors and error correlations (Kulawik et al., 2016).~~ Of course also other sources of uncertainty are relevant in this context, in particular time dependent atmospheric transport and varying biogenic CO₂ contributions (e.g., Houweling et al., 2015, and references given therein).

We conclude that inferring COVID-19 related information on regional-scale CO₂ emissions using current (quite sparse) satellite XCO₂ retrievals requires, if at all possible, a more sophisticated analysis method including the use of detailed *a priori* information and atmospheric transport modelling.

The extent to which COVID-19 related emission reductions can be resolved on smaller scales - such as power plants or cities (e.g., Nassar et al., 2017; Reuter et al., 2019; Zheng et al., 2020a; Wu et al., 2020) has not yet been investigated in detail ~~(to the best of our knowledge)~~this study. For this purpose, XCO₂ retrievals from NASA's OCO-3 mission are ~~also very~~ promising, especially because of its Snapshot Area Map (SAM) mode, which permits the mapping of XCO₂ over ~80 km by 80 km areas around localized anthropogenic CO₂ emission sources (see <https://ocov3.jpl.nasa.gov/> (last access: 28-Aug-2020)). Even more complete coverage is planned for the Copernicus CO2M mission in the future (e.g., Janssens-Maenhout et al., 2020).

Acknowledgements

600 This study has been funded in parts by the European Space Agency (ESA) via projects ICOVAC (Impacts of COVID-19 lockdown measures on Air quality and Climate) and GHG-CCI+ (<http://cci.esa.int/ghg>, last access: 13-August-2020) and the University and the State of Bremen. We acknowledge financial support for the generation of several data sets used as input for this study: (i) European Commission via Copernicus Climate Change Service (C3S, <https://climate.copernicus.eu/>, last access: 22-July-2020) project C3S_312b_Lot2, (ii) the Japanese space agency JAXA (contract 19RT000692) and (iii) 605 EUMETSAT (contract EUM/CO/19/4600002372/RL). H.Boe., Univ. Leicester, was funded as part of NERC’s support of the National Centre for Earth Observation (NE/R016518/1).

We also acknowledge access to OCO-2 XCO₂ data product “OCO2_L2_Lite_FP 10r” obtained from NASA’s Earthdata GES DISC website (<https://disc.gsfc.nasa.gov/datasets?keywords=OCO-2%20v10r&page=1> (last access: 15-Aug-2020)).

We thank JAXA and the National Institute for Environmental Studies (NIES), Japan, for access to GOSAT Level 1 (L1) data 610 and ESA for making the GOSAT L1 products available via the ESA Third Party Mission (TPM) archive.

We acknowledge CarbonTracker CT2019 results provided by NOAA ESRL, Boulder, Colorado, USA, from the website at <http://carbontracker.noaa.gov> (last access: 22-July-2020). We also acknowledge feedback from Andy Jacobson on an early draft of this manuscript.

Some of the work reported here was conducted by the Jet Propulsion Laboratory, California Institute of Technology under 615 contract to NASA. Government sponsorship is acknowledged.

Author contributions

M.B. designed the study, performed the analysis and led the writing of this paper in close cooperation with M.R., S.N., B.F.A., H.B., J.P.B., O.S. K.B. and M.H. Input data and corresponding advice has been provided by M.R., S.N., A.D.N., 620 H.Boe., L.W., J. L., I.A., C.W.O’D. and D.C. All authors contributed to significantly improve the manuscript.

Data availability. The key results of this study are listed in this manuscript in numerical form (Tab. 4). Access information for the satellite data used as input for this study is provided in Tab. 1. The CT2019 data are available from NOAA (see access information given in Tab. 2).

625

Competing financial interests

The authors declare no competing financial interests.

Appendix A

- 630 As explained in the main text, a second method has been applied to the CT2019 and the satellite data. This method is called “Target minus Surrounding” (TmS) and differs from the DAM method in the approach to determine the XCO_2 background. Whereas the DAM method computes the (daily) background as the median of the XCO_2 values in latitude bands, the TmS background is computed from the XCO_2 values in an area surrounding the target region (the coordinates are listed in Tab. 3).
- 635 The TmS results are discussed in the main text. Here we only show three figures. Figure A1 is the same as Fig. 2 but using the TmS method instead of the DAM method. Figure A2 is the TmS version of Fig. 7 and Fig. A3 is the TmS version of Fig. 13.

640

References

645

Agusti-Panareda, A., Diamantakis, M., Massart, S., Chevallier, F., Muñoz-Sabater, J., Barré, J., Curcoll, R., Engelen, R., Langerock, B., Law, R. M., Loh, Z., Morguí, J. A., Parrington, M., Peuch, V.-H., Ramonet, M., Roehl, C., Vermeulen, A. T., Warneke, T., and Wunch, D.: Modelling CO₂ weather – why horizontal resolution matters, *Atmos. Chem. Phys.*, **19**, 7347–7376, <https://doi.org/10.5194/acp-19-7347-2019>, 2019.

650

Basu, S., Guerlet, S., Butz, A., Houweling, S., Hasekamp, O., Aben, I., Krummel, P., Steele, P., Langenfelds, R., Torn, M., Biraud, S., Stephens, B., Andrews, A., and Worthy, D.: Global CO₂ fluxes estimated from GOSAT retrievals of total column CO₂, *Atmos. Chem. Phys.*, **13**, 8695–8717, doi:10.5194/acp-13-8695-2013, 2013.

Boesch, H., Anand, J., and Di Noia, A.: Product User Guide and Specification (PUGS) – ANNEX A for products

CO₂_GOS_OCFP, CH₄_GOS_OCFP & CH₄_GOS_OCPR (v7.2, 2009-2018), 3-Nov-2019, pp. 33, http://wdc.dlr.de/C3S_312b_Lot2/Documentation/GHG/PUGS/C3S_D312b_Lot2.3.2.3-v1.0_PUGS-GHG_ANNEX-A_v3.1.pdf (last access: 17-Aug-2020), 2019.

Bovensmann, H., Burrows, J. P., Buchwitz, M., Frerick, J., Noël, S., Rozanov, V. V., Chance, K. V., and Goede, A. H. P.: SCIAMACHY - Mission objectives and measurement modes, *J. Atmos. Sci.*, **56** (2), 127-150, 1999.

655

Bovensmann, H., M. Buchwitz, J. P. Burrows, M. Reuter, T. Krings, K. Gerilowski, O. Schneising, J. Heymann, A. Tretner, and J. Erzinger, A remote sensing technique for global monitoring of power plant CO₂ emissions from space and related applications, *Atmos. Meas. Tech.*, **3**, 781-811, 2010.

Broquet, G., F.-M. Breon, E. Renault, M. Buchwitz, M. Reuter, H. Bovensmann, F. Chevallier, L. Wu, and P. Ciais, The potential of satellite spectro-imagery for monitoring CO₂ emissions from large cities, *Atmos. Meas. Tech.*, **11**, 681-708,

660

<https://doi.org/10.5194/amt-11-681-2018>, 2018.

Buchwitz, M., Reuter, M., Bovensmann, H., Pillai, D., Heymann, J., Schneising, O., Rozanov, V., Krings, T., Burrows, J. P., Boesch, H., Gerbig, C., Meijer, Y., and Loeschner, A.: Carbon Monitoring Satellite (CarbonSat): assessment of atmospheric CO₂ and CH₄ retrieval errors by error parameterization, *Atmos. Meas. Tech.*, **6**, 3477-3500, 2013.

Buchwitz, M., Reuter, M., Schneising, O., Boesch, H., Guerlet, S., Dils, B., Aben, I., Armante, R., Bergamaschi, P.,

665

Blumenstock, T., Bovensmann, H., Brunner, D., Buchmann, B., Burrows, J. P., Butz, A., Chédin, A., Chevallier, F., Crevoisier, C. D., Deutscher, N. M., Frankenberg, C., Hase, F., Hasekamp, O. P., Heymann, J., Kaminski, T., Laeng, A., Lichtenberg, G., De Mazière, M., Noël, S., Notholt, J., Orphal, J., Popp, C., Parker, R., Scholze, M., Sussmann, R., Stiller, G. P., Warneke, T., Zehner, C., Bril, A., Crisp, D., Griffith, D. W. T., Kuze, A., O'Dell, C., Oshchepkov, S., Sherlock, V., Suto, H., Wennberg, P., Wunch, D., Yokota, T., and Yoshida, Y.: The Greenhouse Gas Climate Change Initiative (GHG-

CCI): comparison and quality assessment of near-surface-sensitive satellite-derived CO₂ and CH₄ global data sets, *Remote Sensing of Environment*, 162, 344-362, doi:10.1016/j.rse.2013.04.024, 2015.

Buchwitz, M., Reuter, M., Schneising, O., Hewson, W., Detmers, R. G., Boesch, H., Hasekamp, O. P., Aben, I., Bovensmann, H., Burrows, J. P., Butz, A., Chevallier, F., Dils, B., Frankenberg, C., Heymann, J., Lichtenberg, G., De Maziere, M., Notholt, J., Parker, R., Warneke, T., Zehner, C., Griffith, D. W. T., Deutscher, N. M., Kuze, A., Suto, H., and Wunch, D.: Global satellite observations of column-averaged carbon dioxide and methane: The GHG-CCI XCO₂ and XCH₄ CRDP3 data set, *Remote Sensing of Environment* 203, 276-295, <http://dx.doi.org/10.1016/j.rse.2016.12.027>, 2017a.

Buchwitz, M., Schneising, O., Reuter, M., Heymann, J., Krautwurst, S., Bovensmann, H., Burrows, J. P., Boesch, H., Parker, R. J., Somkuti, P., Detmers, R. G., Hasekamp, O. P., Aben, I., Butz, A., Frankenberg, C., Turner, A. J., Satellite-derived methane hotspot emission estimates using a fast data-driven method, *Atmos. Chem. Phys.*, 17, 5751-5774, doi:10.5194/acp-17-5751-2017, 2017b.

Buchwitz, M., Reuter, M., Schneising, O., Noel, S., Gier, B., Bovensmann, H., Burrows, J. P., Boesch, H., Anand, J., Parker, R. J., Somkuti, P., Detmers, R. G., Hasekamp, O. P., Aben, I., Butz, A., Kuze, A., Suto, H., Yoshida, Y., Crisp, D., and O'Dell, C.: Computation and analysis of atmospheric carbon dioxide annual mean growth rates from satellite observations during 2003-2016, *Atmos. Chem. Phys.*, 18, 17355-17370, <https://doi.org/10.5194/acp-18-17355-2018>, 2018.

Burrows, J. P., Hölzle, E., Goede, A. P. H., Visser, H., and Fricke, W.: SCIAMACHY—Scanning Imaging Absorption Spectrometer for Atmospheric Chartography, *Acta Astronaut.*, 35(7), 445–451, doi:10.1016/0094-5765(94)00278-t, 1995.

Butz, A., Guerlet, S., Hasekamp, O., Schepers, D., Galli, A., Aben, I., Frankenberg, C., Hartmann, J.-M., Tran, H., Kuze, A., Keppel-Aleks, G., Toon, G., Wunch, D., Wennberg, P., Deutscher, N., Griffith, D., Macatangay, R., Messerschmidt, J., Notholt, J., and Warneke, T.: Toward accurate CO₂ and CH₄ observations from GOSAT, *Geophys. Res. Lett.*, doi:10.1029/2011GL047888, 2011.

Chevallier, F.: On the parallelization of atmospheric inversions of CO₂ surface fluxes within a variational framework, *Geosci. Model. Dev.*, 6, 783-790, doi:10.5194/gmd-6-783-2013, 2013.

Chevallier, F., Palmer, P. I., Feng, L., Boesch, H., O'Dell, C. W., and Bousquet, P.: Towards robust and consistent regional CO₂ flux estimates from in situ and space-borne measurements of atmospheric CO₂, *Geophys. Res. Lett.*, 41, 1065–1070, doi:10.1002/2013GL058772, 2014.

Chevallier, F.: On the statistical optimality of CO₂ atmospheric inversions assimilating CO₂ column retrievals, *Atmos. Chem. Phys.*, 15, 11133–11145, <https://doi.org/10.5194/acp-15-11133-2015>, 2015.

[Chevallier, F., Zheng, B., Broquet, G., Ciais, P., Liu, Z., Davis, S. J., Deng, Z., Wang, Y., Bréon, F.-M., and O'Dell, C. W.: Local anomalies in the column-averaged dry air mole fractions of carbon dioxide across the globe during the first months of the coronavirus recession. *Geophysical Research Letters*, 47, e2020GL090244, <https://doi.org/10.1029/2020GL090244>, 2020.](#)

Ciais, P., Dolman, A. J., Bombelli, A., Duren, R., Peregon, A., Rayner, P. J., Miller, C., Gobron, N., Kinderman, G., Marland, G., Gruber, N., Chevallier, F., Andres, R. J., Balsamo, G., Bopp, L., Bréon, F.-M., Broquet, G., Dargaville, R., Battin, T. J., Borges, A., Bovensmann, H., Buchwitz, M., Butler, J., Canadell, J. G., Cook, R. B., DeFries, R., Engelen, R., Gurney, K. R., Heinze, C., Heimann, M., Held, A., Henry, M., Law, B., Luyssaert, S., Miller, J., Moriyama, T., Moulin, C., Myneni, R. B., Nussli, C., Obersteiner, M., Ojima, D., Pan, Y., Paris, J.-D., Piao, S. L., Poulter, B., Plummer, S., Quegan, S., Raymond, P., Reichstein, M., Rivier, L., Sabine, C., Schimel, D., Tarasova, O., Valentini, R., Wang, R., van der Werf, G., Wickland, D., Williams, M., and Zehner, C.: Current systematic carbon-cycle observations and the need for implementing a policy-relevant carbon observing system, *Biogeosciences*, 11, 3547–3602, <https://doi.org/10.5194/bg-11-3547-2014>, 2014.

Ciais, P., Crisp, D., Denier van der Gon, H., Engelen, R., Janssens-Maenhout, G., Heimann, H., Rayner, P., and Scholze, M.: Towards a European Operational Observing System to Monitor Fossil CO₂ emissions, Final Report from the expert group, European Commission, October 2015, pp. 68, https://edgar.jrc.ec.europa.eu/news_docs/CO2_report_22-10-2015.pdf (last access: 26-Aug-2020), 2015.

Cogan, A. J., Boesch, H., Parker, R. J., Feng, L., Palmer, P. I., Blavier, J.-F. L., Deutscher, N. M., Macatangay, R., Notholt, J., Roehl, C., Warneke, T., and Wunsch, D.: Atmospheric carbon dioxide retrieved from the Greenhouse gases Observing SATellite (GOSAT): Comparison with ground-based TCCON observations and GEOS-Chem model calculations, *J. Geophys. Res.*, 117, D21301, doi:10.1029/2012JD018087, 2012.

Crisp, D., Atlas, R. M., Bréon, F.-M., Brown, L. R., Burrows, J. P., Ciais, P., Connor, B. J., Doney, S. C., Fung, I. Y., Jacob, D. J., Miller, C. E., O'Brien, D., Pawson, S., Randerson, J. T., Rayner, P., Salawitch, R. S., Sander, S. P., Sen, B., Stephens, G. L., Tans, P. P., Toon, G. C., Wennberg, P. O., Wofsy, S. C., Yung, Y. L., Kuang, Z., Chudasama, B., Sprague, G., Weiss, P., Pollock, R., Kenyon, D., and Schroll, S.: The Orbiting Carbon Observatory (OCO) mission, *Advances in Space Research*, 34, 700–709, 2004.

Crisp, D., Meijer, Y., Munro, R., Bowman, K., Chatterjee, A., Baker, D., Chevallier, F., Nassar, R., Palmer, P. I., Agustí-Panareda, A., Al-Saadi, J., Ariel, Y., Basu, S., Bergamaschi, P., Boesch, H., Bousquet, P., Bovensmann, H., Bréon, F.-M., Brunner, D., Buchwitz, M., Buisson, F., Burrows, J. P., Butz, A., Ciais, P., Clerbaux, C., Counet, P., Crevoisier, C., Crowell, S., DeCola, P. L., Deniel, C., Dowell, M., Eckman, R., Edwards, D., Ehret, G., Eldering, A., Engelen, R., Fisher, B., Germain, S., Hakkarainen, J., Hilsenrath, E., Holmlund, K., Houweling, S., Hu, H., Jacob, D., Janssens-Maenhout, G., Jones, D., Jouglet, D., Kataoka, F., Kiel, M., Kulawik, S. S., Kuze, A., Lachance, R. L., Lang, R., Landgraf, J., Liu, J., Liu, Y., Maksyutov, S., Matsunaga, T., McKeever, J., Moore, B., Nakajima, M., Natraj, V., Nelson, R. R., Niwa, Y., Oda, T., O'Dell, C. W., Ott, L., Patra, P., Pawson, S., Payne, V., Pinty, B., Polavarapu, S. M., Retscher, R., Rosenberg, R., Schuh, A., Schwandner, F. M., Shiomi, K., Su, W., Tamminen, J., Taylor, T. E., Veefkind, P., Veihermann, B., Wofsy, S., Worden, J., Wunch, D., Yang, D., Zhang, P., and Zehner, C.: A CONSTELLATION ARCHITECTURE FOR MONITORING CARBON DIOXIDE AND METHANE FROM SPACE, Prepared by the CEOS Atmospheric Composition Virtual

Formatiert: Schriftart: +Textkörper (Times New Roman),
Schriftfarbe: Text 1

- Constellation Greenhouse Gas Team, Committee on Earth Observation Satellites, Version 1.0, 8 October 2018, pp. 173,
[http://ceos.org/document_management/Meetings/Plenary/32/documents/CEOS_AC-](http://ceos.org/document_management/Meetings/Plenary/32/documents/CEOS_AC-VC_White_Paper_Version_1_20181009.pdf)
735 [VC_White_Paper_Version_1_20181009.pdf](http://ceos.org/document_management/Meetings/Plenary/32/documents/CEOS_AC-VC_White_Paper_Version_1_20181009.pdf) (last access: 26-Aug-2020), 2018.
- Eldering, A., Wennberg, P. O., Crisp, D., Schimel, D. S., Gunson, M. R., Chatterjee, A., Liu, J., Schwandner, F. M., Sun, Y.,
O'Dell, C. W., Frankenberg, C., Taylor, T., Fisher, B., Osterman, G. B., Wunch, D., Hakkarainen, J., Tamminen, J., and
305 Weir, B.: The Orbiting Carbon Observatory-2 early science investigations of regional carbon dioxide fluxes, *Science*,
358, eaam5745, doi: 10.1126/science.aam5745, 2017.
- 740 ESA, 2019: ESA, European Space Agency, Copernicus CO₂ Monitoring Mission Requirements Document, version 2.0 of
27/09/19, ESA Earth and Mission Science Division document ref. EOP-SM/3088/YM-ym,
https://esamultimedia.esa.int/docs/EarthObservation/CO2M_MRD_v2.0_Issued20190927.pdf (last access: 15-July-2020),
pp. 82, 2019.
- ESA-NASA-JAXA, 2020: ESA, NASA and JAXA COVID-10 Dashboard (see: <https://www.nasa.gov/coronavirus>,
745 <https://www.nasa.gov/press-release/nasa-partner-space-agencies-amass-global-view-of-covid-19-impacts> and/or
https://www.esa.int/ESA_Multimedia/Images/2020/06/COVID-19_Earth_Observation_Dashboard2, last access: 15-July-
2020).
- Dils, B. Buchwitz, M., Reuter, M., Schneising, O., Boesch, H. , Parker, R., Guerlet, S., Aben, I., Blumenstock, T., Burrows,
J. P., Butz, A., Deutscher, N. M., Frankenberg, C., Hase, F., Hasekamp, O. P., Heymann, J., De Maziere, M., Notholt, J.,
750 Sussmann, R., Warneke, T., Griffith, D., Sherlock, V., and Wunch, D.: The Greenhouse Gas Climate Change Initiative
(GHG-CCI): comparative validation of GHG-CCI SCIAMACHY/ENVISAT and TANSO-FTS/GOSAT CO₂ and CH₄
retrieval algorithm products with measurements from the TCCON, *Atmos. Meas. Tech.*, 7, 1723-1744, 2014.
- Friedlingstein, P., Jones, M. W., O'Sullivan, M., Andrew, R. M., Hauck, J., Peters, G. P., Peters, W., Pongratz, J., Sitch, S.,
Le Quéré, C., Bakker, D. C. E., Canadell, J. G., Ciais, P., Jackson, R. B., Anthoni, P., Barbero, L., Bastos, A., Bastrikov, V.,
755 Becker, M., Bopp, L., Buitenhuis, E., Chandra, N., Chevallier, F., Chini, L. P., Currie, K. I., Feely, R. A., Gehlen, M.,
Gilfillan, D., Gkritzalis, T., Goll, D. S., Gruber, N., Gutekunst, S., Harris, I., Haverd, V., Houghton, R. A., Hurtt, G., Ilyina,
T., Jain, A. K., Joetzjer, E., Kaplan, J. O., Kato, E., Klein Goldewijk, K., Korsbakken, J. I., Landschützer, P., Lauvset, S. K.,
Lefèvre, N., Lenton, A., Lienert, S., Lombardozzi, D., Marland, G., McGuire, P. C., Melton, J. R., Metzl, N., Munro, D. R.,
Nabel, J. E. M. S., Nakaoka, S. I., Neill, C., Omar, A. M., Ono, T., Peregon, A., Pierrot, D., Poulter, B., Rehder, G.,
760 Resplandy, L., Robertson, E., Rödenbeck, C., Séférian, R., Schwinger, J., Smith, N., Tans, P. P., Tian, H., Tilbrook, B.,
Tubiello, F. N., van der Werf, G. R., Wiltshire, A. J., and Zaehle, S.: Global Carbon Budget 2019, *Earth Syst. Sci. Data*, 11,
1783-1838, doi: 10.5194/essd-11-1783-2019, 2019.

Gier, B. K., Buchwitz, M., Reuter, M., Cox, P. M., Friedlingstein, P., and Eyring, V.: Spatially resolved evaluation of Earth system models with satellite column-averaged CO₂, *Biogeosciences Discuss.*, **17**, 6115–6144, <https://doi.org/10.5194/bg-17-6115-2020>, 2020.

Hakkarainen, J., Ialongo, I., and Tamminen, J.: Direct space-based observations of anthropogenic CO₂ emission areas from OCO-2, *Geophys. Res. Lett.*, **43**, 11,400–11,406, doi:10.1002/2016GL070885, 2016.

Hakkarainen, J., Ialongo, I., Maksyutov, S., and Crisp, D.: Analysis of Four Years of Global XCO₂ Anomalies as Seen by Orbiting Carbon Observatory-2, *Remote Sensing*, **11**, 850, doi:10.3390/rs11070850, pp. 20, 2019.

Houweling, S., Baker, D., Basu, S., Boesch, H., Butz, A., Chevallier, F., Deng, F., Dlugokencky, E. J., Feng, L., Ganshin, A., Hasekamp, O., Jones, D., Maksyutov, S., Marshall, J., Oda, T., O'Dell, C. W., Oshchepkov, S., Palmer, P. I., Peylin, P., Poussi, Z., Reum, F., Takagi, H., Yoshida, Y., and Zhuralev, R.: An intercomparison of inverse models for estimating sources and sinks of CO₂ using GOSAT measurements, *J. Geophys. Res. Atmos.*, **120**, 5253–5266, doi:10.1002/2014JD022962, 2015.

IPCC: Climate Change 2013: The Physical Science Basis, Working Group I Contribution to the Fifth Assessment Report of the Intergovernmental Report on Climate Change, <http://www.ipcc.ch/report/ar5/wg1/> (last access: 21-February-2019), Cambridge University Press, 2013.

Jacobson, A. R., Schuldt, K. N., Miller, J. B., Oda, T., Tans, P., Andrews, A., Mund, J., Ott, L., Collatz, G. J., Aalto, T., Afshar, S., Aikin, K., Aoki, S., Apadula, F., Baier, B., Bergamaschi, P., Beyersdorf, A., Biraud, S. C., Bollenbacher, A., Bowling, D., Brailsford, G., Abshire, J. B., Chen, G., Chen, H., Chmura, L., Colomb, A., Conil, S., Cox, A., Cristofanelli, P., Cuevas, E., Curcoll, R., Sloop, C. D., Davis, K., Wekker, S. D., Delmotte, M., DiGangi, J. P., Dlugokencky, E., Ehleringer, J., Elkins, J. W., Emmenegger, L., Fischer, M. L., Forster, G., Frumau, A., Galkowski, M., Gatti, L. V., Gloor, E., Griffis, T., Hammer, S., Haszpra, L., Hatakka, J., Heliasz, M., Hensen, A., Hermanssen, O., Hints, E., Holst, J., Jaffe, D., Karion, A., Kawa, S. R., Keeling, R., Keronen, P., Kolari, P., Kominkova, K., Kort, E., Krummel, P., Kubistin, D., Labuschagne, C., Langenfelds, R., Laurent, O., Laurila, T., Lauvaux, T., Law, B., Lee, J., Lehner, I., Leuenberger, M., Levin, I., Levula, J., Lin, J., Lindauer, M., Loh, Z., Lopez, M., Lund Myhre, C., Machida, T., Mammarella, I., Manca, G., Manning, A., Manning, A., Marek, M. V., Marklund, P., Martin, M. Y., Matsueda, H., McKain, K., Meijer, H., Meinhardt, F., Miles, N., Miller, C. E., Mölder, M., Montzka, S., Moore, F., Morgui, J.-A., Morimoto, S., Munger, B., Necki, J., Newman, S., Nichol, S., Niwa, Y., O'Doherty, S., Ottosson-Löfvenius, M., Paplawsky, B., Peischl, J., Peltola, O., Pichon, J.-M., Piper, S., Plass-Dölmer, C., Ramonet, M., Reyes-Sanchez, E., Richardson, S., Riris, H., Ryerson, T., Saito, K., Sargent, M., Sasakawa, M., Sawa, Y., Say, D., Scheeren, B., Schmidt, M., Schmidt, A., Schumacher, M., Shepson, P., Shook, M., Stanley, K., Steinbacher, M., Stephens, B., Sweeney, C., Thoning, K., Torn, M., Turnbull, J., Tørseth, K., Bulk, P. V. D., Laan-Luijckx, I. T. V. D., Dinter, D. V., Vermeulen, A., Viner, B., Vitkova, G., Walker, S., Weyrauch, D., Wofsy, S., Worthy, D., Young, D., and Zimnoch, M.: CarbonTracker CT2019, DOI: 10.25925/39m3-6069, 2020.

Formatiert: Schriftart: Times New Roman, Englisch (Vereinigtes Königreich)

Formatiert: Schriftart: Times New Roman, Englisch (Vereinigtes Königreich)

Formatiert: Schriftart: Times New Roman, Englisch (Vereinigtes Königreich), Nicht Hochgestellt/ Tiefgestellt

Formatiert: Schriftart: Times New Roman, Englisch (Vereinigtes Königreich)

Formatiert: Schriftart: Times New Roman, Englisch (Vereinigtes Königreich)

Formatiert: Schriftart: Times New Roman, Englisch (Vereinigtes Königreich)

Formatiert: Schriftart: Times New Roman, Englisch (Vereinigtes Königreich), Nicht Hochgestellt/ Tiefgestellt

Formatiert: Schriftart: Times New Roman, Englisch (Vereinigtes Königreich)

- 795 Janssens-Maenhout, G., Pinty, B., Dowell, M., Zunker, H., Andersson, E., Balsamo, G., Bezy, J.-L., Brunhes, T., Boesch, H.,
Bojkov, B., Brunner, D., Buchwitz, M., Crisp, D., Ciais, P., Counet, P., Dee, D., Denier van der Gon, H., Dolman, H.,
Drinkwater, M., Dubovik, O., Engelen, R., Fehr, T., Fernandez, V., Heimann, M., Holmlund, K., Houweling, S., Husband,
R., Juvyns, O., Kentarchos, A., Landgraf, J., Lang, R., Loeschner, A., Marshall, J., Meijer, Y., Nakajima, M., Palmer, P. I.,
Peylin, P., Rayner, P., Scholze, M., Sierk, B., Tamminen, J., and Veefkind P.: Towards an operational anthropogenic CO₂
800 emissions monitoring and verification support capacity, *Bulletin of the American Meteorological Society (BAMS)*,
10.1175/BAMS-D-19-0017.1, <https://doi.org/10.1175/BAMS-D-19-0017.1>, Published Online: 10 February 2020, 2020.
- Kaminski, T., Scholze, M., Voßbeck, M., Knorr, W., Buchwitz, M., and Reuter, M.: Constraining a terrestrial biosphere
model with remotely sensed atmospheric carbon dioxide, *Remote Sensing of Environment* 203, 109-124, 2017.
- Kiel, M., O'Dell, C. W., Fisher, B., Eldering, A., Nassar, R., MacDonald, C. G., and Wennberg, P. O.: How bias correction
805 goes wrong: measurement of XCO₂ affected by erroneous surface pressure estimates, *Atmos. Meas. Tech.*, 12, 2241–2259,
<https://doi.org/10.5194/amt-12-2241-2019>, 2019.
- Kuhlmann, G., Broquet, G., Marshall, J., Clément, V., Löschner, A., Meijer, Y., and Brunner, D.: Detectability of CO₂
emission plumes of cities and power plants with the Copernicus Anthropogenic CO₂ Monitoring (CO2M) mission, *Atmos.*
Meas. Tech., 12, 6695-6719, doi: 10.5194/amt-12-6695-2019, 2019.
- 810 Kulawik, S., Wunch, D., O'Dell, C., Frankenberg, C., Reuter, M., Oda, T., Chevallier, F., Sherlock, V., Buchwitz, M.,
Osterman, G., Miller, C. E., Wennberg, P. O., Griffith, D., Morino, I., Dubey, M. K., Deutscher, N. M., Notholt, J., Hase, F.,
Warneke, T., Susstmann, R., Robinson, J., Strong, K., Schneider, M., De Maziere, M., Shiomi, K., Feist, D. G., Iraci, L. T.,
Wolf, J.: Consistent evaluation of ACOS-GOSAT, BESD-SCIAMACHY, CarbonTracker, and MACC through comparisons
to TCCON, *Atmos. Meas. Tech.*, 9, 683-709, doi:10.5194/amt-9-683-2016, 2016.
- 815 Kuze, A., Suto, H., Shiomi, K., Kawakami, S., Tanaka, M., Ueda, Y., Deguchi, A., Yoshida, J., Yamamoto, Y., Kataoka, F.,
Taylor, T. E., and Buijs, H. L.: Update on GOSAT TANSO-FTS performance, operations, and data products after more than
6 years in space, *Atmos. Meas. Tech.*, 9, 2445-2461, doi:10.5194/amt-9-2445-2016, 2016.
- Labzovskii, L. D., Jeong, S.-J., and Parazoo, N. C.: Working towards confident spaceborne monitoring of carbon emissions
from cities using Orbiting Carbon Observatory-2, *Remote Sensing of Environment*, 233, 111359, doi:
820 10.1016/j.rse.2019.111359, 2019.
- Lauer, A., Eyring, V., Righi, M., Buchwitz, M., Defourny, P., Evaldsson, M., Friedlingstein, P., de Jeu, R., de Leeuw, G.,
Loew, A., Merchant, C. J., Müller, B., Popp, T., Reuter, M., Sandven, S., Senfleben, D., Stengel, M., Van Roozendaal, M.,
Wenzel, S., and Willén, U.: Benchmarking CMIP5 models with a subset of ESA CCI Phase 2 data using the ESMValTool,
Remote Sensing of Environment, 203, 9-39, <http://dx.doi.org/10.1016/j.rse.2017.01.007>, 2017.

- 825 [Lespinas, F., Wang, Y., Broquet, G., Breon, F.-M., Buchwitz, M., Reuter, M., Meijer, Y., Loeschner, A., Janssens-Maenhout, G., Zheng, B., and Ciais, P.: The potential of a constellation of low earth orbit satellite imagers to monitor worldwide fossil](#)
[fuel CO₂ emissions from large cities and point sources. *Carbon Balance Manage* 15, 18, pp. 12,](#)
<https://doi.org/10.1186/s13021-020-00153-4> (last access: 1-Feb-2021), 2020.
- Le Quéré, C., Andrew, R. M., Friedlingstein, P., Sitch, S., Pongratz, J., Manning, A. C., Korsbakken, J. I., Peters, G. P.
- 830 Canadell, J. G., Jackson, R. B., Boden, T. A., Tans, P. P., Andrews, O. D., Arora, V. K., Bakker, D. D. E., Barbero, L.,
Becker, M., Betts, R. A., Bopp, L., Chevallier, F., Chini, L. P., Ciais, P., Cosca, C. E., Cross, J., Currie, K., Gasser, T.,
Harris, I., Hauck, J., Haverd, V., Houghton, R. A., Hunt, C. W., Hurtt, G., Ilyina, T., Jain, A. K., Kato, E., Kautz, M.,
Keeling, R. F., Goldewijk, K. K., Körtzinger, A., Landschützer, P., Lefèvre, N., Lenton, A., Lienert, S., Lima, I.,
Lombardozzi, D., Metzl, N., Millero, F., Monteiro, P. M. S., Munro, D. R., Nabel, J. E. M. S., Nakaoka, S., Nojiri, Y., Padín,
835 X. A., Peregon, A., Pfeil, B., Pierrot, D., Poulter, B., Rehder, G., Reimer, J., Rödenbeck, C., Schwinger, J., Séférian, R.,
Skjelvan, I., Stocker, B. D., Tian, H., Tilbrook, B., van der Laan-Luijkx, I. T., van der Werf, G. R., van Heuven, S., Viovy,
N., Vuichard, N., Walker, A. P., Watson, A. J., Wiltshire, A. J., Zaehle, S., and Zhu, D.: Global Carbon Budget 2017, *Earth*
System Science Data, 10, 405-448, DOI: 10.5194/essd-10-405-2018, 2018.
- Le Quéré, C., Jackson, R. B., Jones, M. W., Smith, A. J. P., Abernethy, S., Andrew, R. M., De-Gol, A. J., Willis, D. R.,
- 840 Shan, Y., Canadell, J. G., Friedlingstein, P., Creutzig, G. and Peters, G. P.: Temporary reduction in daily global CO₂
emissions during the COVID-19 forced confinement. *Nat. Clim. Chang.* **10**, 647–653, [https://doi.org/10.1038/s41558-020-](https://doi.org/10.1038/s41558-020-0797-x)
[0797-x](https://doi.org/10.1038/s41558-020-0797-x) (last access: 15-July-2020), 2020.
- Liu, J., Bowman, K. W., Schimel, D. S., Parazoo, N. C., Jiang, Z., Lee, M., Bloom, A. A., Wunch, D., Frankenberg, C., Sun,
Y., O'Dell, C. W., Gurney, K. R., Menemenlis, D., Gierach, M., Crisp, D., and Eldering, A.: Contrasting carbon cycle
845 responses of the tropical continents to the 2015–2016 El Niño, *Science*, 358, eaam5690, pp. 7, 2017.
- Liu, Z., Ciais, P., Deng, Z., Lei, R., Davis, S. J., Feng, S., Zheng, B., Cui, D., Dou, X., He, P., Zhu, B., Lu, C., Ke, P., Sun,
T., Wang, Y., Yue, X., Wang, Y., Lei, Y., Zhou, H., Cai, Z., Wu, Y., Guo, R., Han, T., Xue, J., Boucher, O., Boucher, E.,
Chevallier, F., Wei, Y., Zhong, H., Kang, C., Zhang, N., Chen, B., Xi, F., Marie, F., Zhang, Q., Guan, D., Gong, P.,
Kammen, D. M., He, K., and Schellnhuber, H. J., <https://arxiv.org/abs/2004.13614> (last access: 15-July-2020), in review.;
- 850 [Near-real-time-data captured record decline in global CO₂ emissions due to COVID-19,](#)
<https://arxiv.org/ftp/arxiv/papers/2004/2004.13614.pdf> (last access: 5-Jan-2021), pp. 45, 2020.
- Massart, S., Agusti-Panareda, A., Heymann, J., Buchwitz, M., Chevallier, F., Reuter, M., Hilker, M., Burrows, J. P.,
Deutscher, N. M., Feist, D. G., Hase, F., Sussmann, R., Desmet, F., Dubey, M. K., Griffith, D. W. T., Kivi, R., Petri, C.,
Schneider, M., and Velasco, V. A.: Ability of the 4-D-Var analysis of the GOSAT BESD XCO₂ retrievals to characterize
855 atmospheric CO₂ at large and synoptic scales, *Atmos. Chem. Phys.*, 16, 1653-1671, doi:10.5194/acp-16-1653-2016, 2016.

Matsunaga, T., and Maksyutov, S. (eds.): A Guidebook on the Use of Satellite Greenhouse Gases Observation Data to Evaluate and Improve Greenhouse Gas Emission Inventories, Satellite Observation Center, National Institute for Environmental Studies, Japan, 1st Edition, March 2018, pp. 137,
https://www.nies.go.jp/soc/doc/GHG_Satellite_Guidebook_1st_12d.pdf (last access: 26-Aug-2020), 2018.

860 Miller, S. M., Michalak, A. M., Detmers, R. G., Hasekamp, O. P., Bruhwiler, L. M. P., and Schwietzke, S.: China's coal mine methane regulations have not curbed growing emissions, *Nature Communications*, volume 10, article number: 303, 2019.

Miller, S. M. and Michalak, A. M.: The impact of improved satellite retrievals on estimates of biospheric carbon balance, *Atmos. Chem. Phys.*, 20, 323–331, <https://doi.org/10.5194/acp-20-323-2020>, 2020.

865 Nassar, R., Hill, T. G., McLinden, C. A., Wunch, D., Jones, D. B. A., and Crisp, D.: Quantifying CO₂ emissions from individual power plants from space. *Geophysical Research Letters*, 44, 10,045– 10,053.
<https://doi.org/10.1002/2017GL074702>, 2017.

Noël, S., et al.: XCO₂ retrieval for GOSAT and GOSAT-2 based on the FOCAL algorithm, manuscript in preparation, 2020-Reuter, M., Buchwitz, M., Borchardt, J., Hilker, M., Bovensmann, H., Burrows, J. P., Di Noia, A., Suto, H., Yoshida,
 870 Y., Buschmann, M., Deutscher, N. M., Feist, D. G., Griffith, D. W. T., Hase, F., Kivi, R., Morino, I., Notholt, J., Ohyama, H., Petri, C., Podolske, J. R., Pollard, D. F., Sha, M. K., Shiomi, K., Sussmann, R., Te, Y., Velazco, V. A., and Warneke, T.: XCO₂ retrieval for GOSAT and GOSAT-2 based on the FOCAL algorithm, *Atmos. Meas. Tech. Discuss.*,
<https://doi.org/10.5194/amt-2020-453>, in review, 2020.

O'Dell, C. W., Connor, B., Bösch, H., O'Brien, D., Frankenberg, C., Castano, R., Christi, M., Eldering, D., Fisher, B.,
 875 Gunson, M., McDuffie, J., Miller, C. E., Natraj, V., Oyafuso, F., Polonsky, I., Smyth, M., Taylor, T., Toon, G. C., Wennberg, P. O., and Wunch, D.: The ACOS CO₂ retrieval algorithm – Part 1: The ACOS CO₂ retrieval algorithm – Part 1: Description and validation against synthetic observations, *Atmos. Meas. Tech.*, 5, 99–121, doi:10.5194/amt-5-99-2012, 2012.

O'Dell, C. W., Eldering, A., Wennberg, P. O., Crisp, D., Gunson, M. R., Fisher, B., Frankenberg, C., Kiel, M., Lindqvist, H., Mandrake, L., Merrelli, A., Natraj, V., Nelson, R. R., Osterman, G. B., Payne, V. H., Taylor, T. R., Wunch, D., Drouin, B. J.,
 880 Oyafuso, F., Chang, A., McDuffie, J., Smyth, M., Baker, D. F., Basu, S., Chevallier, F., Crowell, S. M. R., Feng, L., Palmer, P. I., Dubey, M., García, O. E., 15 Griffith, D. W. T., Hase, F., Iraci, L. T., Kivi, R., Morino, I., Notholt, J., Ohyama, H., Petri, C., Roehl, C. M., Sha, M. K., Strong, K., Sussmann, R., Te, Y., Uchino, O., and Velazco, V. A.: Improved Retrievals of Carbon Dioxide from the Orbiting Carbon Observatory-2 with the version 8 ACOS algorithm, *Atmos. Meas. Tech.*, 11, 6539–6576, <https://doi.org/10.5194/amt-11-6539-2018>, 2018.

885 Osterman, G., O'Dell, C., Eldering, A., Fisher, B., Crisp, D., Cheng, C., Frankenberg, C., Lambert, A., Gunson, M., Mandrake, L., Wunch, D.: Orbiting Carbon Observatory-2 & 3 (OCO-2 & OCO-3) Data Product User's Guide, Operational

Level 2 Data Versions 10 and Lite File Version 10 and VEarly, Technical Report National Aeronautics and Space Administration, Jet Propulsion Laboratory, California Institute of Technology, Pasadena, California, USA, Version 1.0, Revision A, June 8, 2020, Data Release: 10 (OCO-2), VEarly (OCO-3),

890 https://docserver.gesdisc.eosdis.nasa.gov/public/project/OCO/OCO2_OCO3_B10_DUG.pdf (last access: 17-Aug-2020), 2020.

Palmer, P. I., Feng, L., Baker, D., Chevallier, F., Bösch, H., and Somkuti, P.: Net carbon emissions from African biosphere dominate pan-tropical atmospheric CO₂ signal, *Nature Communications* 10, Article number: 3344, pp. 9, <https://www.nature.com/articles/s41467-019-11097-w> (last access: 15-July-2020), 2019.

895 Peters, W., Jacobson, A. R., Sweeney, C., Andrews, A. E., Conway, T. J., Masarie, K., Miller, J. B., Bruhwiler, L. M. P., Pétron, G., Hirsch, A. I., Worthy, D. E. J., van der Werf, G. R., Randerson, J. T., Wennberg, P. O., Krol, M. C., and Tans, P. P.: An atmospheric perspective on North American carbon dioxide exchange: CarbonTracker, *Proceedings of the National Academy of Sciences (PNAS) of the United States of America*, 104, 18925–18930, doi:10.1073/pnas.0708986104, 2007.

Pillai, D., M. Buchwitz, C. Gerbig, T. Koch, M. Reuter, H. Bovensmann, J. Marshall, J. P. Burrows, Tracking city CO₂

900 emissions from space using a high resolution inverse modeling approach: A case study for Berlin, Germany, *Atmos. Chem. Phys.*, 16, 9591-9610, doi:10.5194/acp-16-9591-2016, 2016.

Pinty, B., Janssens-Maenhout, G., Dowell, M., Zunker, H., Brunhes, T., Ciais, P., Dee, D., Denier van der Gon, H., Dolman, H., Drinkwater, M., Engelen, R., Heimann, M., Holmlund, K., Husband, R., Kentarchos, A., Meijer, Y., Palmer, P., and Scholze, M.: An Operational Anthropogenic CO₂ Emissions Monitoring & Verification Support capacity - Baseline

905 Requirements, Model Components and Functional Architecture, doi: 10.2760/39384, European Commission Joint Research Centre, EUR 28736 EN, pp. 102, https://www.copernicus.eu/sites/default/files/2019-09/CO2_Red_Report_2017.pdf (last access: 26-Aug-2020), 2017.

Pinty, B., Ciais, P., Dee, D., Dolman, H., Dowell, M., Engelen, R., Holmlund, K., Janssens-Maenhout, G., Meijer, Y., Palmer, P., Scholze, M., Denier van der Gon, H., Heimann, M., Juvyns, O., Kentarchos, A., and Zunker, H.: An Operational

910 Anthropogenic CO₂ Emissions Monitoring & Verification Support Capacity – Needs and high level requirements for in situ measurements, doi: 10.2760/182790, European Commission Joint Research Centre, EUR 29817 EN, pp. 77, https://www.copernicus.eu/sites/default/files/2019-09/CO2_Green_Report_2019.pdf (last access: 26-Aug-2020), 2019.

Reuter, M., Buchwitz, M., Schneising, O., Heymann, J., Bovensmann, H., and Burrows, J. P.: A method for improved SCIAMACHY CO₂ retrieval in the presence of optically thin clouds, *Atmos. Meas. Tech.*, 3, 209-232, 2010.

915 Reuter, M., Bovensmann, H., Buchwitz, M., Burrows, J. P., Connor, B. J., Deutscher, N. M., Griffith, D. W. T., Heymann, J., Keppel-Aleks, G., Messerschmidt, J., Notholt, J., Petri, C., Robinson, J., Schneising, O., Sherlock, V., Velazco, V., Warneke, W., Wennberg, P. O., and Wunch, D.: Retrieval of atmospheric CO₂ with enhanced accuracy and precision from

SCIAMACHY: Validation with FTS measurements and comparison with model results, *J. Geophys. Res.*, 116, D04301, doi:10.1029/2010JD015047, 2011.

920 Reuter, M., Buchwitz, M., Schneising, O., Hase, F., Heymann, J., Guerlet, S., Cogan, A. J., Bovensmann, H., and Burrows, J. P.: A simple empirical model estimating atmospheric CO₂ background concentrations, *Atmos. Meas. Tech.*, 5, 1349-1357, 2012.

Reuter, M., Boesch, H., Bovensmann, H., Bril, A., Buchwitz, M., Butz, A., Burrows, J. P., O'Dell, C. W., Guerlet, S., Hasekamp, O., Heymann, J., Kikuchi, N., Oshchepkov, S., Parker, R., Pfeifer, S., Schneising, O., Yokota, T., and Yoshida, Y.: A joint effort to deliver satellite retrieved atmospheric CO₂ concentrations for surface flux inversions: the ensemble median algorithm EMMA, *Atmos. Chem. Phys.*, 13, 1771-1780, 2013.

925 Reuter, M., Buchwitz, M., Hilker, M., Heymann, J., Schneising, O., Pillai, D., Bovensmann, H., Burrows, J. P., Bösch, H., Parker, R., Butz, A., Hasekamp, O., O'Dell, C. W., Yoshida, Y., Gerbig, C., Nehrkorn, T., Deutscher, N. M., Warneke, T., Notholt, J., Hase, F., Kivi, R., Sussmann, R., Machida, T., Matsueda, H., and Sawa, Y.: Satellite-inferred European carbon sink larger than expected, *Atmos. Chem. Phys.*, 14, 13739-13753, 2014a.

Reuter, M., Buchwitz, M., Hilboll, A., Richter, A., Schneising, O., Hilker, M., Heymann, J., Bovensmann, H., and Burrows, J. P.: Decreasing emissions of NO_x relative to CO₂ in East Asia inferred from satellite observations, *Nature Geoscience*, 28 Sept. 2014, doi:10.1038/ngeo2257, pp. 4, 2014b.

Reuter, M., Buchwitz, M., Schneising, O., Noël, S., Rozanov, V., Bovensmann, H., and Burrows, J. P.: A Fast Atmospheric Trace Gas Retrieval for Hyperspectral Instruments Approximating Multiple Scattering - Part 1: Radiative Transfer and a Potential OCO-2 XCO₂ Retrieval Setup, *Remote Sens.*, 9, 1159, doi:10.3390/rs9111159, 2017a.

Reuter, M., Buchwitz, M., Schneising, O., Noël, S., Bovensmann, H., and Burrows, J. P.: A Fast Atmospheric Trace Gas Retrieval for Hyperspectral Instruments Approximating Multiple Scattering - Part 2: Application to XCO₂ Retrievals from OCO-2, *Remote Sens.*, 9, 1102, doi:10.3390/rs9111102, 2017b.

940 Reuter, M., Buchwitz, M., Hilker, M., Heymann, J., Bovensmann, H., Burrows, J. P., Houweling, S., Liu, Y., Nassar, R., Chevallier, F., Ciais, P., Marshall, J., and Reichstein, M.: How much CO₂ is taken up by the European terrestrial biosphere? *Bull. Amer. Meteor. Soc.* doi:10.1175/BAMS-D-15-00310.1, 24 April 2017, 665-671, 2017c.

Reuter, M., Buchwitz, M., Schneising, O., Krautwurst, S., O'Dell, C. W., Richter, A., Bovensmann, H., and Burrows, J. P.: Towards monitoring localized CO₂ emissions from space: co-located regional CO₂ and NO₂ enhancements observed by the OCO-2 and SSP satellites, *Atmos. Chem. Phys.*, <https://www.atmos-chem-phys.net/19/9371/2019/>, 19, 9371-9383, 2019.

945 Reuter, M., Buchwitz, M., Schneising, O., Noel, S., Bovensmann, H., Burrows, J. P., Boesch, H., Di Noia, A., Anand, J., Parker, R. J., Somkuti, P., Wu, L., Hasekamp, O. P., Aben, I., Kuze, A., Suto, H., Shiomi, K., Yoshida, Y., Morino, I., Crisp, D., O'Dell, C. W., Notholt, J., Petri, C., Warneke, T., Velazco, V. A., Deutscher, N. M., Griffith, D. W. T., Kivi, R., Pollard,

D. F., Hase, F., Sussmann, R., Te, Y. V., Strong, K., Roche, S., Sha, M. K., De Maziere, M., Feist, D. G., Iraci, L. T., Roehl,
950 C. M., Retscher, C., and Schepers, D.: Ensemble-based satellite-derived carbon dioxide and methane column-averaged dry-
air mole fraction data sets (2003-2018) for carbon and climate applications, *Atmos. Meas. Tech.*, 13, 789-819,
<https://doi.org/10.5194/amt-13-789-2020>, 2020.

Rodgers, C. D., *Inverse Methods for Atmospheric Sounding: Theory and Practice*, World Scientific Publishing, 2000.

Schneising, O., Buchwitz, M., Burrows, J. P., Bovensmann, H., Reuter, M., Notholt, J., Macatangay, R., and Warneke, T.:
955 Three years of greenhouse gas column-averaged dry air mole fractions retrieved from satellite – Part 1: Carbon dioxide,
Atmos. Chem. Phys., 8, 3827–3853, <https://doi.org/10.5194/acp-8-3827-2008>, 2008.

Schneising, O., Heymann, J., Buchwitz, M., Reuter, M., Bovensmann, H., and Burrows, J. P.: Anthropogenic carbon dioxide
source areas observed from space: assessment of regional enhancements and trends, *Atmos. Chem. Phys.*, 13, 2445-2454,
doi:10.5194/acp-13-2445-2013, 2013.

960 Schneising, O., Reuter, M., Buchwitz, M., Heymann, J., Bovensmann, H., and Burrows, J. P.: Terrestrial carbon sink
observed from space: variation of growth rates and seasonal cycle amplitudes in response to interannual surface temperature
variability, *Atmos. Chem. Phys.*, 14, 133-141, 2014.

Schwandner, F. M., Gunson, M. R., Miller, C. E., Carn, S. A., Eldering, A., Krings, T., Verhulst, K. R., Schimel, D. S.,
Nguyen, H. M., Crisp, D., O'Dell, C. W., Osterman, G. B., Iraci, L. T., and Podolske, J. R.: Spaceborne detection of
965 localized carbon dioxide sources, *Science*, 358, eaam5782, doi: 10.1126/science.aam5782, 2017.

Sussmann, R., and Rettinger, M.: Can We Measure a COVID-19-Related Slowdown in Atmospheric CO₂ Growth?
Sensitivity of Total Carbon Column Observations, *Remote Sens.*, 12, 2387, <https://www.mdpi.com/2072-4292/12/15/2387>
(last access: 5-Oct-2020), 2020.

[Tohjima, Y., Patra, P.K., Niwa, Y., Mukai, H., Sasakawa, M., and Machida, T.: Detection of fossil-fuel CO₂ plummet in](#)
970 [China due to COVID-19 by observation at Hateruma, *Sci Rep* 10, 18688, <https://doi.org/10.1038/s41598-020-75763-6>, 2020.](#)

Veefkind, J. P., Aben, I., McMullan, K., Förster, H., De Vries, J., Otter, G., Claas, J., Eskes, H. J., De Haan, J. F., Kleipool,
Q., Van Weele, M., Hasekamp, O., Hoogeveen, R., Landgraf, J., Snel, R., Tol, P., Ingmann, P., Voors, R., Kruizinga, B.,
Vink, R., Visser, H., and Levelt, P. F.: TROPOMI on the ESA Sentinel-5 Precursor: A GMES mission for global
observations of the atmospheric composition for climate, air quality and ozone layer applications. *Rem. Sens. Environment*,
975 120:70–83, 2012.

Velasco, V. A., M. Buchwitz, H. Bovensmann, M. Reuter, O. Schneising, J. Heymann, T. Krings, K. Gerilowski, and J. P.
Burrows, Towards space based verification of CO₂ emissions from strong localized sources: fossil fuel power plant
emissions as seen by a CarbonSat constellation, *Atmos. Meas. Tech.*, 4, 2809-2822, 2011.

Formatiert: Schriftart: Times New Roman, Englisch
(Vereinigtes Königreich)

- Wu, L., Hasekamp, O., Hu, H., Landgraf, J., Butz, A., aan de Brugh, J., Aben, I., Pollard, D. F., Griffith, D. W. T., Feist, D.
980 G., Koshelev, D., Hase, F., Toon, G. C., Ohyama, H., Morino, I., Notholt, J., Shiomi, K., Iraci, L., Schneider, M., de
Mazière, M., Sussmann, R., Kivi, R., Warneke, T., Goo, T.-Y., and Té, Y.: Carbon dioxide retrieval from OCO-2 satellite
observations using the RemoTeC algorithm and validation with TCCON measurements, *Atmos. Meas. Tech.*, 11, 3111–
3130, <https://doi.org/10.5194/amt-11-3111-2018>, 2018.
- Wu, L., Aben, I., and Hasekamp, O. P.: Product User Guide and Specification (PUGS) – ANNEX B for products
985 CO2_GOS_SRFP, CH4_GOS_SRFP (v2.3.8, 2009-2018), 29-Nov-2019, pp. 26,
[http://wdc.dlr.de/C3S_312b_Lot2/Documentation/GHG/PUGS/C3S_D312b_Lot2.3.2.3-v1.0_PUGS-GHG_ANNEX-
B_v3.1.pdf](http://wdc.dlr.de/C3S_312b_Lot2/Documentation/GHG/PUGS/C3S_D312b_Lot2.3.2.3-v1.0_PUGS-GHG_ANNEX-B_v3.1.pdf) (last access: 17-Aug-2020), 2019.
- Wu, D., Lin, J., Oda, T., and Kort, E.: Space-based quantification of per capita CO₂ emissions from cities, *Environ. Res.
Lett.* 15, pp. 9, <https://iopscience.iop.org/article/10.1088/1748-9326/ab68eb/pdf> (last access: 15-July-2020), 2020.
- 990 Wunch, D., Toon, G.C., Wennberg, P.O., Wofsy, S.C., Stephens, B.B., Fischer, M.L., Uchino, O., Abshire, J.B., Bernath, P.,
Biraud, S.C., Blavier, J.-F.L., Boone, C., Bowman, K.P., Browell, E.V., Campos, T., Connor, B.J., Daube, B.C., Deutscher,
N.M., Diao, M., Elkins, J.W., Gerbig, C., Gottlieb, E., Griffith, D.W.T., Hurst, D.F., Jimenez, R., Keppel-Aleks, G., Kort,
E.A., Macatangay, R., Machida, T., Matsueda, H., Moore, F., Morino, I., Park, S., Robinson, J., Roehl, C.M., Sawa, Y.,
Sherlock, V., Sweeney, C., Tanaka, T., Zondlo, M.A.: Calibration of the total carbon column observing network using
995 aircraft profile data. *Atmos. Meas. Tech.* 3:1351–1362. <http://dx.doi.org/10.5194/amt-3-1351-2010>, 2010.
- Wunch, D., Toon, G. C., Blavier, J.-F. L., Washenfelder, R. A., Notholt, J., Connor, B. J., Griffith, D. W. T., Sherlock, V.,
and Wennberg, P. O.: The Total Carbon Column Observing Network. *Phil. Trans. R. Soc. A*, 369, 2087–2112,
doi:10.1098/rsta.2010.0240, 2011.
- Wunch, D., Wennberg, P. O., Osterman, G., Fisher, B., Naylor, B., Roehl, C. M., O'Dell, C., Mandrake, L., Viatte, C., Kiel,
1000 M., Griffith, D. W. T., Deutscher, N. M., Velazco, V. A., Notholt, J., Warneke, T., Petri, C., De Maziere, M., Sha, M. K.,
Sussmann, R., Rettinger, M., Pollard, D., Robinson, J., Morino, I., Uchino, O., Hase, F., Blumenstock, T., Feist, D. G.,
Arnold, S. G., Strong, K., Mendonca, J., Kivi, R., Heikkinen, P., Iraci, L., Podolske, J., Hillyard, P. W., Kawakami, S.,
Dubey, M. K., Parker, H. A., Sepulveda, E., García, O. E., Te, Y., Jeseck, P., Gunson, M. R., Crisp, D., and Eldering, A.:
Comparisons of the Orbiting Carbon Observatory-2 (OCO-2) XCO₂ measurements with TCCON, *Atmos. Meas. Tech.*, 10,
1005 2209-2238, doi:10.5194/amt-10-2209-2017, 2017.
- Wunch, D., Mendonca, J., Colebatch, O., Allen, N. T., Blavier, J.-F., Roche, S., Hedelius, J., Neufeld, G., Springett, S.,
Worthy, D., Kessler, R., and Strong, K.: TCCON data from East Trout Lake, SK (CA), Release GGG2014.R1. TCCON data
archive, hosted by CaltechDATA, <https://doi.org/10.14291/tcon.ggg2014.eastroutlake01.R1>, 2018.

- Ye, X., Lauvaux, T., Kort, E. A., Oda, T., Feng, S., Lin, J. C., Yang, E. G., and Wu, D.: Constraining fossil fuel CO₂ emissions from urban area using OCO-2 observations of total column CO₂, *Journal of Geophysical Research: Atmospheres*, 125, e2019JD030528. <https://doi.org/10.1029/2019JD030528>, 2020.
- Yin, Y., Ciais, P., Chevallier, F., Li, W., Bastos, A., Piao, S., Wang, T., and Liu, H.: Changes in the response of the Northern Hemisphere carbon uptake to temperature over the last three decades. *Geophysical Research Letters*, 45, 4371–4380, <https://doi.org/10.1029/2018GL077316>, 2018-2018to
- Yoshida, Y., Kikuchi, N., Morino, I., Uchino, O., Oshchepkov, S., Bril, A., Saeki, T., Schutgens, N., Toon, G. C., Wunch, D., Roehl, C. M., Wennberg, P. O., Griffith, D. W. T., Deutscher, N. M., Warneke, T., Notholt, J., Robinson, J., Sherlock, V., Connor, B., Rettinger, M., Sussmann, R., Ahonen, P., Heikkinen, P., Kyrö, E., Mendonca, J., Strong, K., Hase, F., Dohe, S., and Yokota, T.: Improvement of the retrieval algorithm for GOSAT SWIR XCO₂ and XCH₄ and their validation using TCCON data, *Atmos. Meas. Tech.*, 6, 1533–1547, doi:10.5194/amt-6-1533-2013, 2013.
- Zhang, R., Zhang, Y., Lin, H., Feng, X., Fu, T.-M., and Wang, Y.: NO_x Emission Reduction and Recovery during COVID-19 in East China, *Atmosphere*, 11, 433, pp. 15, doi:10.3390/atmos11040433, 2020.
- Zheng, B., Chevallier, F., Ciais, P., Broquet, G., Wang, Y., Lian, J., and Zhao, Y.: Observing carbon dioxide emissions over China's cities and industrial areas with the Orbiting Carbon Observatory-2, *Atmos. Chem. Phys. Discuss.*, 20, 8501–8510, <https://doi.org/10.5194/acp-2020-123> (<https://doi.org/10.5194/acp-20-8501-2020> (last access: 15-July-2020), in review, 5-Jan-2021), 2020a.
- Zheng, B., Geng, G., Ciais, P., Davis, S. J., Martin, R. V., Meng, J., Wu, N., Chevallier, F., Broquet, G., Boersma, F., van der A., R., Lin, J., Guan, D., Lei, Y., He, Kebin, K., and Zhang, Q.: Satellite-based estimates of decline and rebound in China's CO₂ emissions during COVID-19 pandemic, <https://arxiv.org/ftp/arxiv/papers/2006/2006.08196.pdf> (last access: 15-July-2020), pp. 46, in review, *Sci. Adv.* 6, eabd4998, <https://advances.sciencemag.org/content/6/49/eabd4998> (last access: 5-Jan-2021), 2020b.
- Zeng, N., Han, P., Liu, D., Liu, Z., Oda, T., Martin, C., Liu, Z., Yao, B., Sun, W., Wang, P., Cai, Q., Dickerson, R., and Maksyutov, S.: Global to local impacts on atmospheric CO₂ caused by COVID-19 lockdown, pp. 20, <https://arxiv.org/abs/2010.13025> (last access: 5-Jan-2021), 2020.

1035

Tables:

Table 1. Overview of the satellite XCO₂ Level 2 (L2) input data products. (#) ~~These products~~Products are available via the Copernicus Climate Data Store (CDS, <https://cds.climate.copernicus.eu/cdsapp#!/dataset/satellite-carbon-dioxide?tab=overview> (last access: 23-September-2020)) ~~currently~~until end of 2019. Year 2020 data will be made available via the CDS in ~~mid~~ 2021 but are ~~also~~ available from the authors on request. ~~(see contact information).~~

1040

Satellite	Algorithm	Product version	Product ID	References	Data provider and data access information
OCO-2	ACOS	v10r	CO2_OC2_ACOS	O'Dell et al., 2018; Kiel et al., 2019; Osterman et al., 2020	Product “OCO2_L2_Lite_FP 10r” obtained from NASA’s Earthdata GES DISC website: https://disc.gsfc.nasa.gov/datasets?keywords=OCO-2%20v10r&page=1 (last access: 15-Aug-2020)
GOSAT	UoL-FP	v7.3	CO2_GOS_OCFP	Cogan et al., 2012; Boesch et al., 2019	Generated by authors (#) Generated by Univ. Leicester (contact: Antonio Di Noia: adn9@leicester.ac.uk) and available via the CDS (#)
GOSAT	RemoTeC	v2.3.8	CO2_GOS_SRFP	Butz et al., 2011; Wu et al., 2019	Generated by authors (#) Generated by SRON (contact: Lianghai Wu: L.Wu@sron.nl) and available via the CDS (#)
GOSAT	FOCAL	v1.0	CO2_GOS_FOCA	Noël et al., 2020	Generated by authors Univ. Bremen and available on request (contact: Stefan Noël: Stefan.Noel@iup.physik.uni-bremen.de)

Table 2. Overview of the CarbonTracker CT2019 data set. For this study we used data from the period January 2015 to December 2018.

Model / Version	Details	Reference	Access
CarbonTracker CT2019	Atmospheric CO ₂ molefraction profiles (spatio-temporal sampling: 3°x2°, 3-hourly) and CO ₂ fluxes (spatio-temporal sampling: 1°x1°, 3-hourly)	Jacobson et al., 2020 DOI: http://dx.doi.org/10.25925/39m3-6069 (last access: 22-July-2020)	CarbonTracker CT2019, http://carbontracker.noaa.gov (last access: 22-July-2020)

Table 3. Corner coordinates of the East China target region as analysed in this study.

Region ID	Comments	Latitude range	Lontitude range
		[deg North]	[deg East]
East China	Target region for DAM and TmS methods	28 – 44	102 – 126
	Extended region for TmS method	18 -54	93 - 135

Formatierte Tabelle

Eingefügte Zellen

Formatiert: Schriftart: Fett

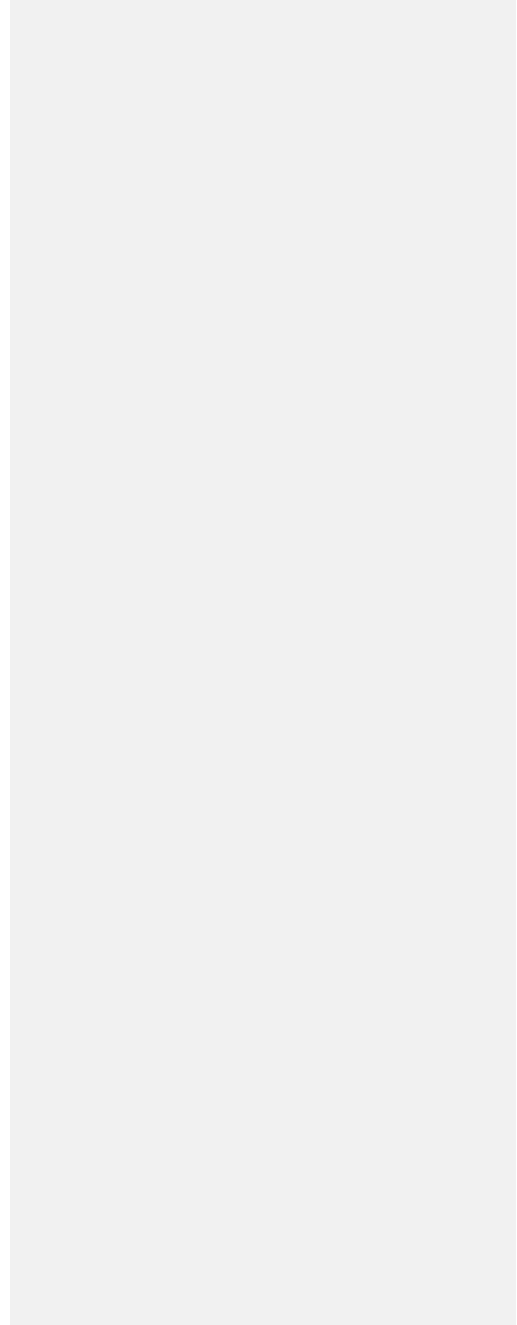
Verbundene Zellen

Table 4. Numerical values of the ensemble-based $\text{AXCO}_2^{\text{FF}}\text{CO}_2^{\text{FFDAMI}}$ results as shown in Fig. 13. Listed are the median values and corresponding 1-sigma uncertainties (in brackets). The dimensionless values listed here represent the relative $\text{AXCO}_2^{\text{FF}}\text{CO}_2^{\text{FFDAMI}}$ change for January-May 2020 relative to October-December 2019 and previous years. The listed data refer to the difference relative to October to December 2019, i.e., the corresponding offset (October to December 2019 mean) has been subtracted. (“OND” anomalies, see main text).

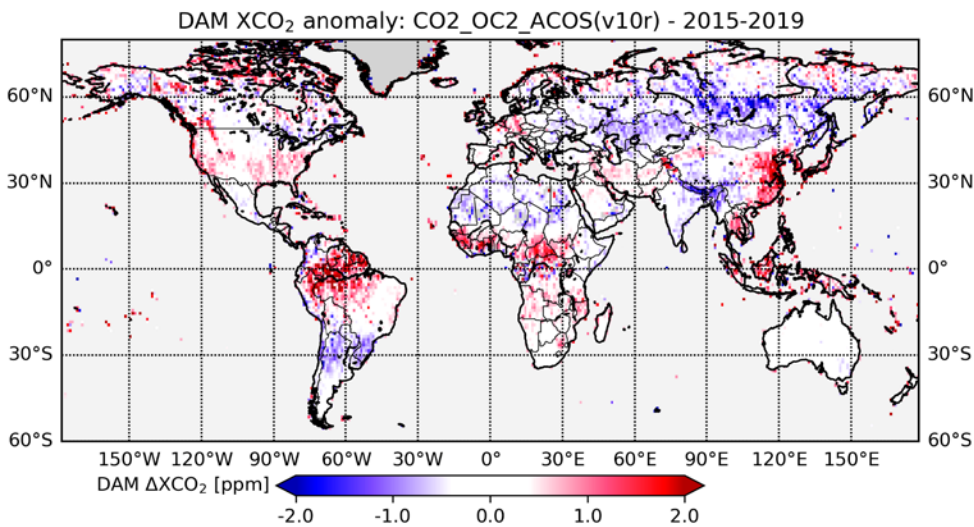
Month	October	November	December	January	February	March	April	May
Product ID	2019	2019	2019	2020	2020	2020	2020	2020
CO2_OC2_ACOS	-0.000004 (0.023025)	0.005001 (0.032024)	-0.005010 (0.018015)	0.015008 (0.029026)	-0.008010 (0.020024)	-0.007003 (0.016020)	-0.018 (0.023 (0.017)	-0.0160 (0.028020)
CO2_GOS_OCFP	-0.084049 (0.077046)	0.025026 (0.074038)	0.058071 (0.053050)	-0.133110 (0.035077)	-0.056055 (0.051087)	-0.151 (0.087101)	-0.242281 (0.034055)	-0.110181 (0.160058)
CO2_GOS_SRFP	-0.067076 (0.039031)	0.130111 (0.045030)	-0.063061 (0.049054)	0.043038 (0.091101)	-0.064 (0.061053)	0.024011 (0.093081)	-0.106082 (0.046059)	0.016024 (0.082027)
CO2_GOS_FOCA	-0.048057 (0.049042)	0.052053 (0.062029)	-0.004008 (0.043040)	-0.041044 (0.042062)	-0.016046 (0.104081)	-0.189176 (0.057066)	-0.040041 (0.079069)	-0.110181 (0.063025)
Ensemble	-0.050047 (0.036031)	0.053048 (0.055047)	-0.004002 (0.049054)	-0.029027 (0.078065)	-0.036021 (0.028050)	-0.081085 (0.105091)	-0.103106 (0.099120)	-0.057028 (0.063075)

[illegible]

|



1070 **Figures:**



Formatiert: Links, Abstand Nach: 0 Pt., Zeilenabstand: einfach

Figure-1

1075 DAM XCO₂ anomaly map at 1°x1° resolution generated from OCO-2 Level 2 XCO₂ (v10r, land) for 2015 to 2019.

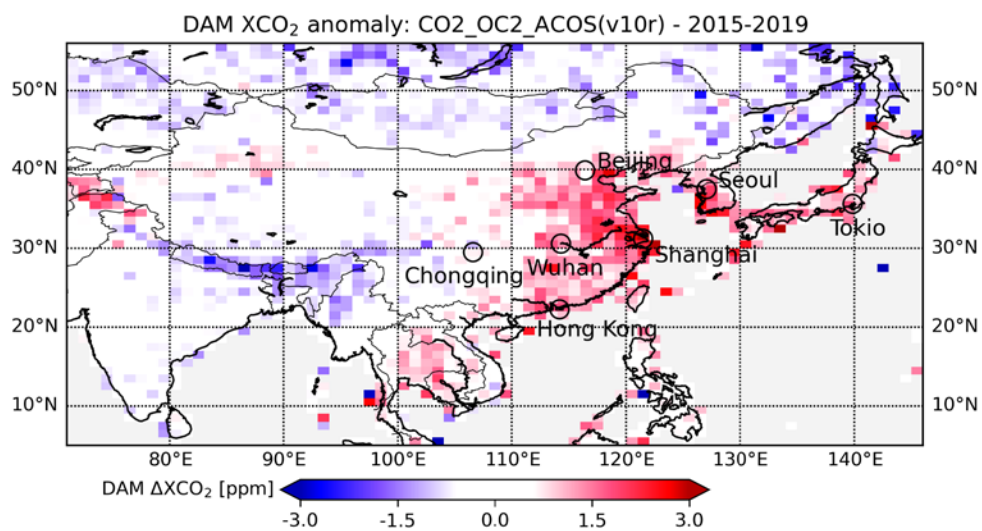
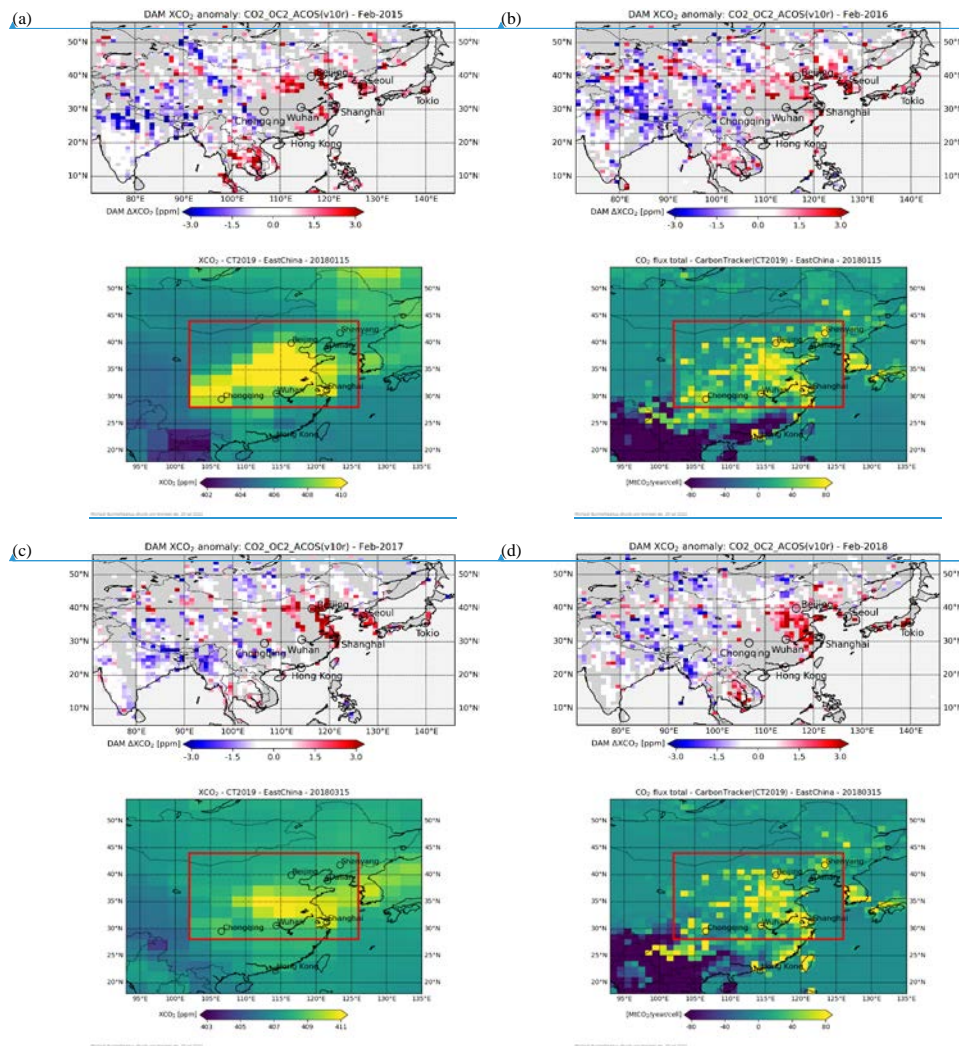


Figure 2: As Fig. 1 but for China and surrounding areas.



Formatiert: Schriftart: Nicht Fett

Formatiert: Beschriftung, Abstand Nach: 6 Pt.,
Zeilenabstand: 1.5 Zeilen

Formatiert: Beschriftung, Zentriert, Abstand Nach: 6 Pt.,
Zeilenabstand: 1.5 Zeilen

Formatiert: Schriftart: Nicht Fett

Formatierte Tabelle

Formatiert: Beschriftung, Abstand Nach: 6 Pt.,
Zeilenabstand: 1.5 Zeilen

Formatiert: Beschriftung, Zentriert, Abstand Nach: 6 Pt.,
Zeilenabstand: 1.5 Zeilen

Formatiert: Schriftart: Nicht Fett

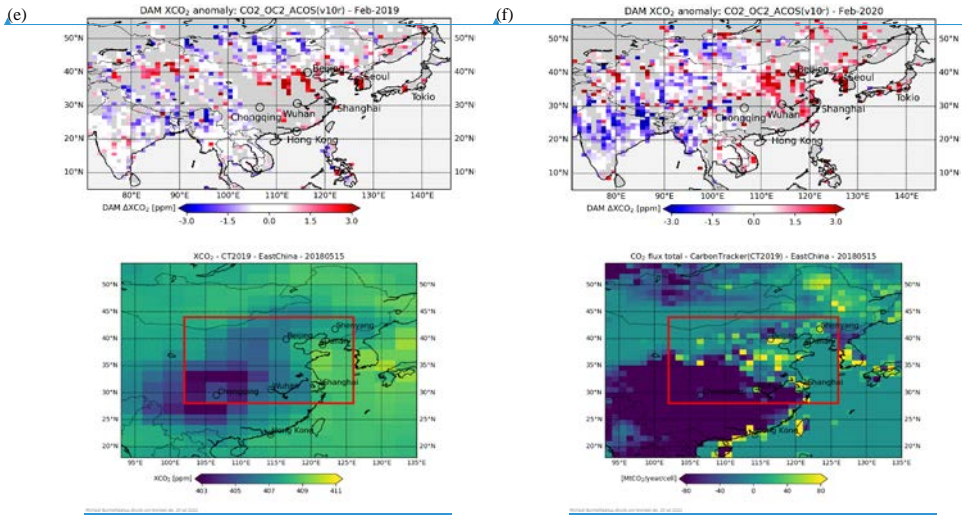
Formatiert: Beschriftung, Abstand Nach: 6 Pt.,
Zeilenabstand: 1.5 Zeilen

Formatiert: Beschriftung, Zentriert, Abstand Nach: 6 Pt.,
Zeilenabstand: 1.5 Zeilen

Formatiert: Schriftart: Nicht Fett

Formatiert: Beschriftung, Abstand Nach: 6 Pt.,
Zeilenabstand: 1.5 Zeilen

Formatiert: Beschriftung, Zentriert, Abstand Nach: 6 Pt.,
Zeilenabstand: 1.5 Zeilen



- Formatiert: Schriftart: Nicht Fett
- Formatiert: Schriftart: Nicht Fett
- Formatiert: Beschriftung, Abstand Nach: 6 Pt., Zeilenabstand: 1.5 Zeilen
- Formatiert: Beschriftung, Zentriert, Abstand Nach: 6 Pt., Zeilenabstand: 1.5 Zeilen
- Formatiert: Beschriftung, Abstand Nach: 6 Pt., Zeilenabstand: 1.5 Zeilen
- Formatiert: Beschriftung, Zentriert, Abstand Nach: 6 Pt., Zeilenabstand: 1.5 Zeilen

- Formatiert: Zeilenabstand: Doppelt

Figure 3: As Fig. 2 but for (a) February 2015 to (f) February 2020.

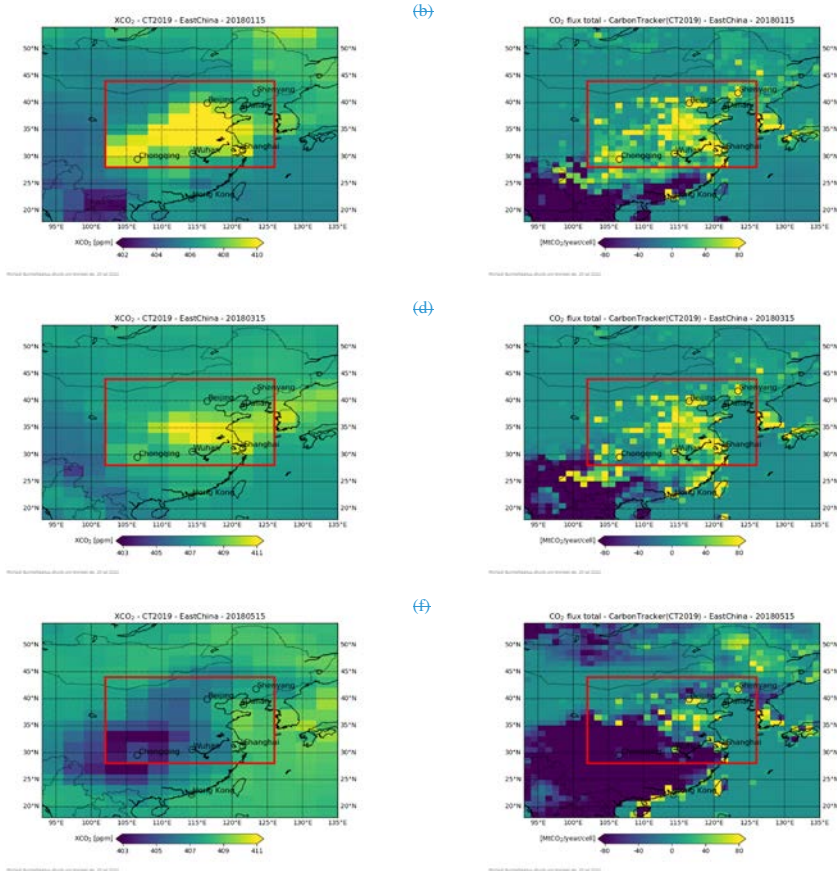
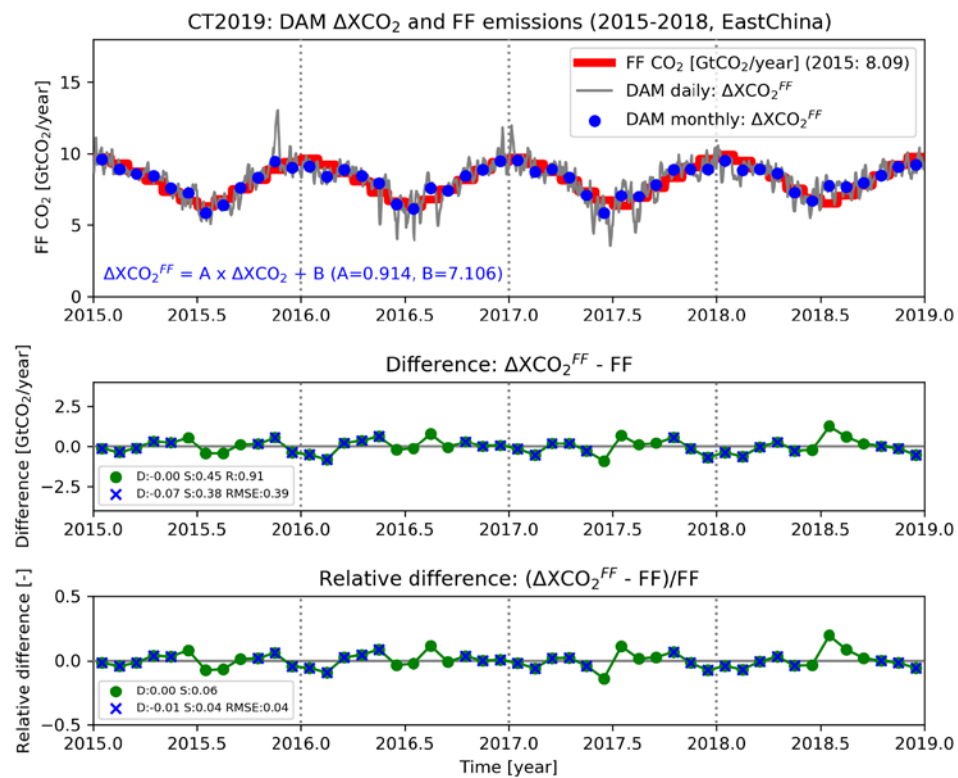
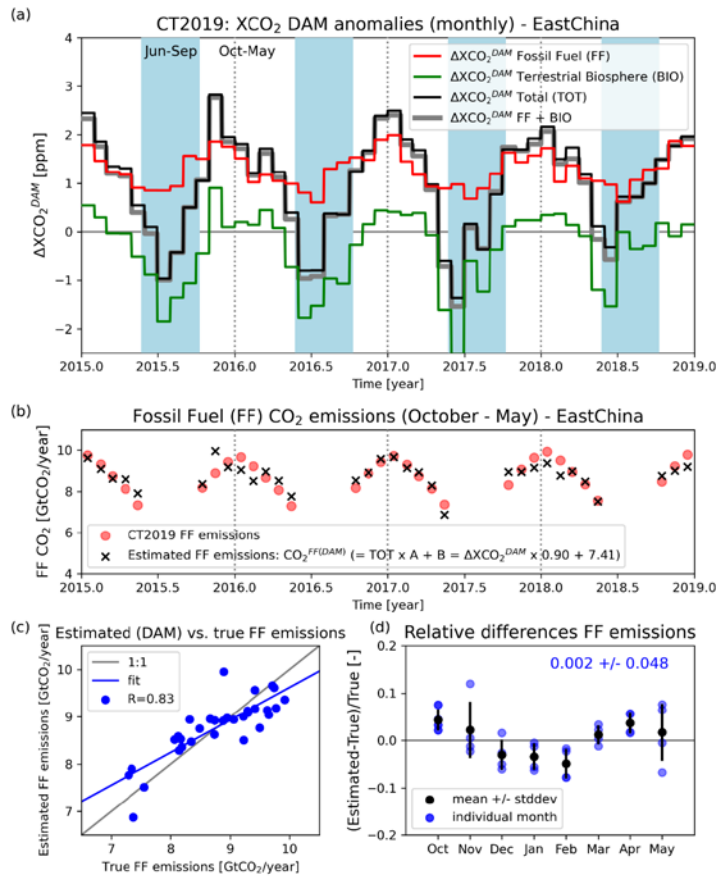


Figure 1: Left: CT2019 XCO₂ (left, in ppm) and corresponding CO₂ surface fluxes (right, in MtCO₂/year/cell) for 15-Jan-2018 (first row), 15-Mar-2018 (middle) and 15-May-2018 (bottom). The red rectangle encloses the East China target region as defined for this study.



Michael.Buchwitz@iup.physik.uni-bremen.de, 20-july-2020



Michael.Buchwitz@ip.physik.uni-bremen.de, 28-january-2021

Figure 52: Results obtained by applying the DAM method to CT2019 XCO₂. **Top panel:** The thick red line shows the CT2019 fossil fuel (FF) monthly CO₂ emissions in GtCO₂/year for target region East China. The thin grey line shows daily $\Delta\text{XCO}_2^{\text{FF}}$. **Different monthly $\Delta\text{XCO}_2^{\text{DAM}}$ components:** Total $\Delta\text{XCO}_2^{\text{DAM}}$ (TOT) and the blue dots show monthly $\Delta\text{XCO}_2^{\text{FF}}$ (see main text for a detailed explanation). **Middle panel:** Absolute difference between monthly $\Delta\text{XCO}_2^{\text{FF}}$ fits FF (red) and the CT2019 FF target region emissions. Listed is the mean difference \bar{D} , the standard deviation of the difference S , the linear correlation coefficient R biogenic (BIO, green) components and the root-mean-square error (RMSE). All quantities (except R) are listed for all months (green dots) and separately for the months their sum (FF + BIO). The non-shaded time periods October to May (blue) indicate the periods analysed in this

publication. (b) East China October to May FF CO₂ emissions (red dots) and estimated emissions CO₂^{FF(DAM)} (black crosses). **Bottom panel: the same** as obtained from total ΔXCO₂^{DAM} (TOT as shown in panel (a)) using the formula shown in (b). (c) Scatter plot of estimated versus true (i.e., CT2019) FF emissions. (d) Relative difference of estimated and true emissions.

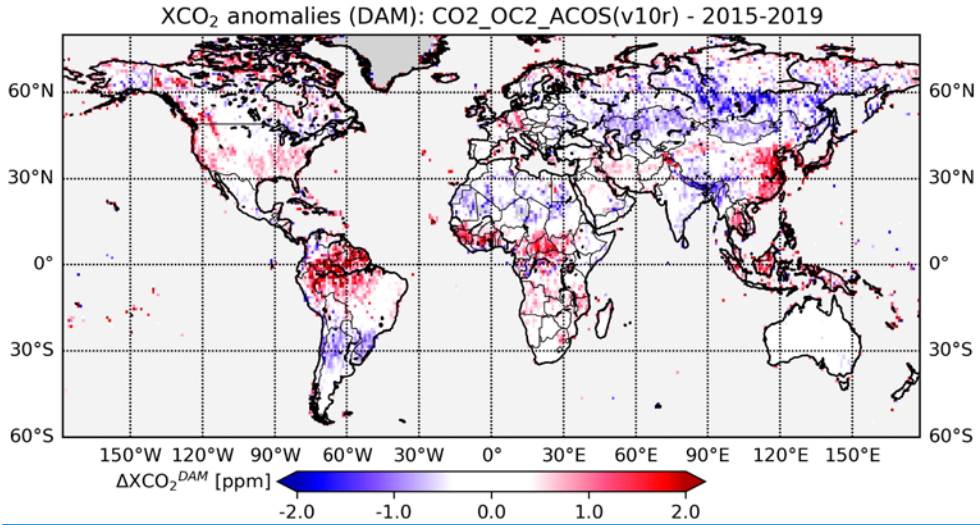


Figure 3: DAM XCO₂ anomaly map at 1° x 1° resolution generated from OCO-2 Level 2 XCO₂ (v10r, land) for 2015 to 2019.

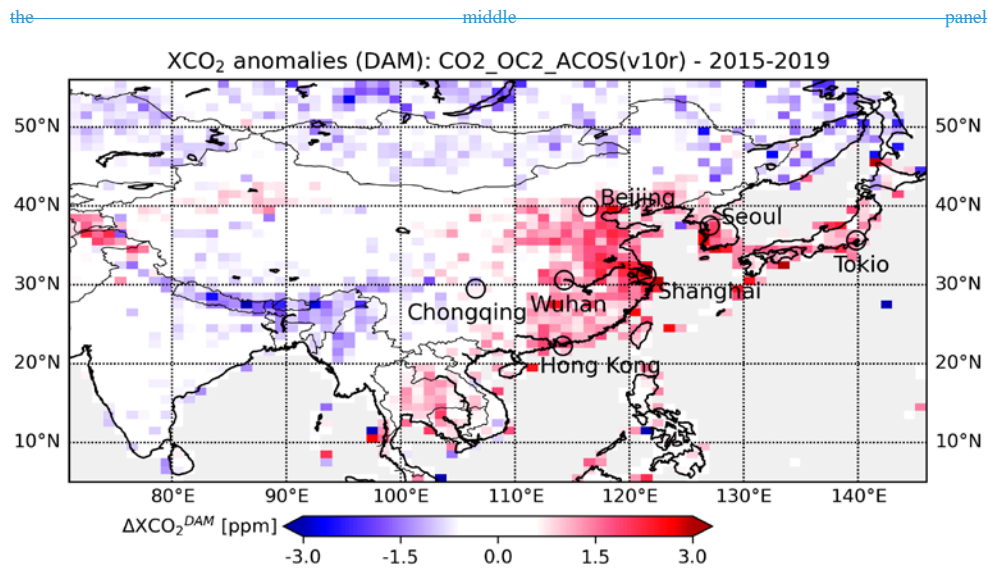


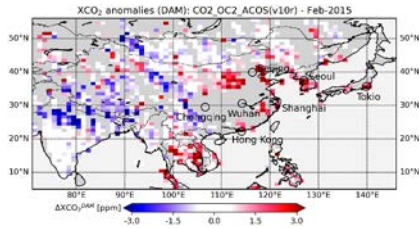
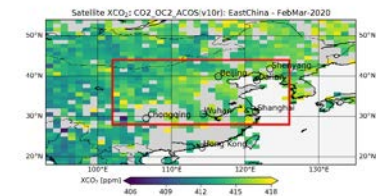
Figure 4: As Fig. 3 but for the relative differences (as fraction, not percent, see panel title) instead of the absolute differences. China and surrounding areas.

Formatiert: Schriftart: 9 Pt., Fett

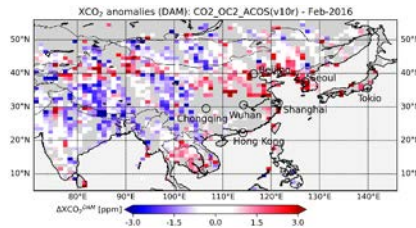
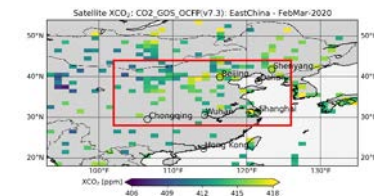
Formatiert: Standard, Abstand Nach: 0 Pt., Zeilenabstand: einfach

Formatiert: Schriftart: 9 Pt., Fett

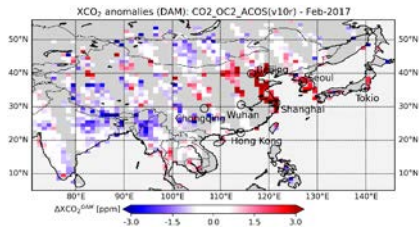
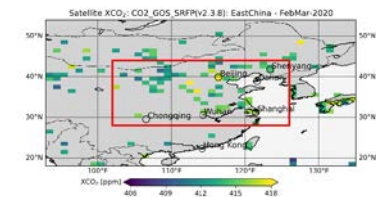
(a)



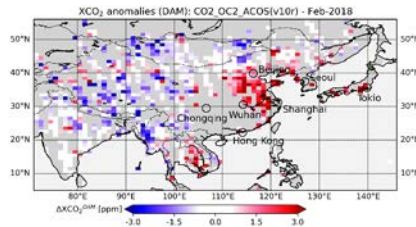
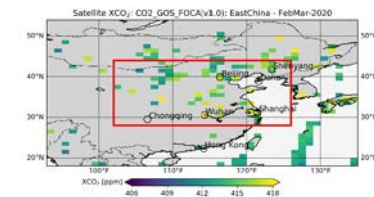
(b)

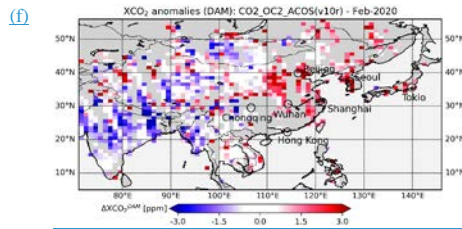
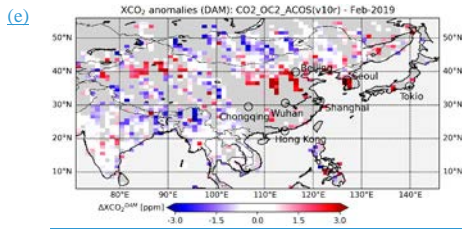


(c)



(d)

**Formatiert:** Schriftart: 10 Pt.**Formatiert:** Standard, Abstand Nach: 0 Pt., Zeilenabstand: einfach**Formatiert:** Standard, Links, Abstand Nach: 0 Pt., Zeilenabstand: einfach**Formatiert:** Schriftart: 10 Pt.**Formatierte Tabelle****Formatiert:** Standard, Abstand Nach: 0 Pt., Zeilenabstand: einfach**Formatiert:** Standard, Links, Abstand Nach: 0 Pt., Zeilenabstand: einfach**Formatiert:** Schriftart: 10 Pt.**Formatiert:** Standard, Abstand Nach: 0 Pt., Zeilenabstand: einfach**Formatiert:** Standard, Links, Abstand Nach: 0 Pt., Zeilenabstand: einfach**Formatiert:** Schriftart: 10 Pt.**Formatiert:** Standard, Abstand Nach: 0 Pt., Zeilenabstand: einfach**Formatiert:** Standard, Links, Abstand Nach: 0 Pt., Zeilenabstand: einfach



Formatiert: Nicht Hervorheben

1125 [Figure 5: As Fig. 4 but for \(a\) February 2015 to \(f\) February 2020.](#)

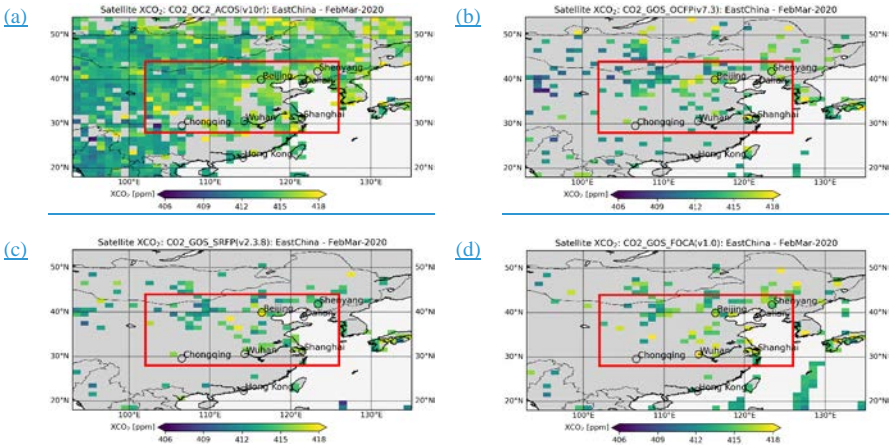
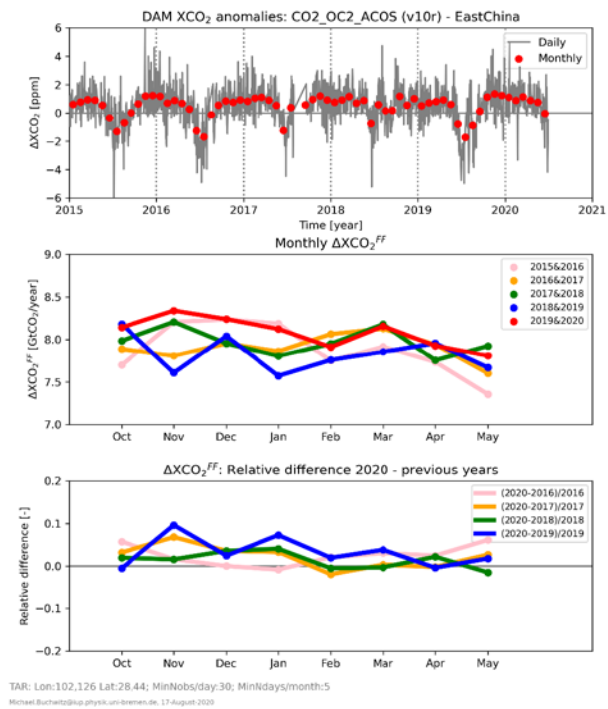


Figure 6: Panel (a): OCO-2 XCO₂ (version 10r, product ID CO2_OC2_ACOS) over land at 1°x1° resolution for February-March 2020. The red rectangle encloses the investigated East China target region. Panels (b)-(d) as panel (a) but for products CO2_GOS_OCFP (b), CO2_GOS_SRFP (c), and CO2_GOS_FOCA (d) (see Tab. 1 for details).



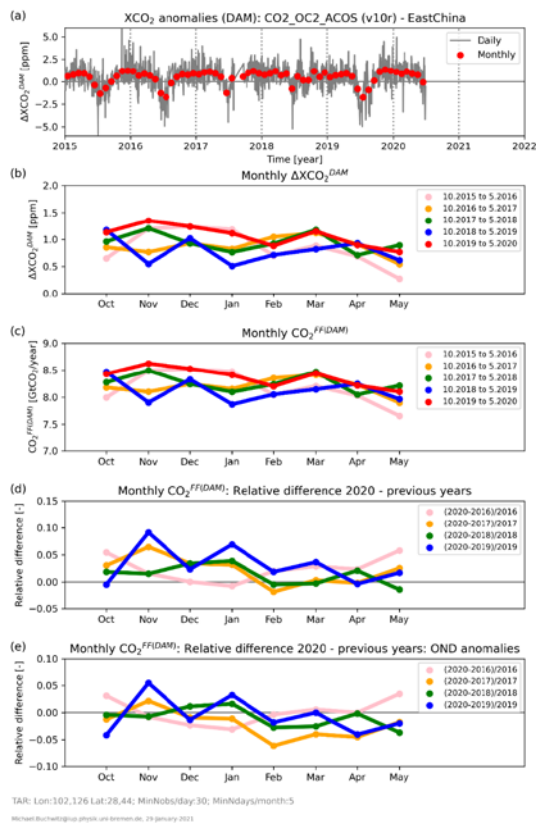
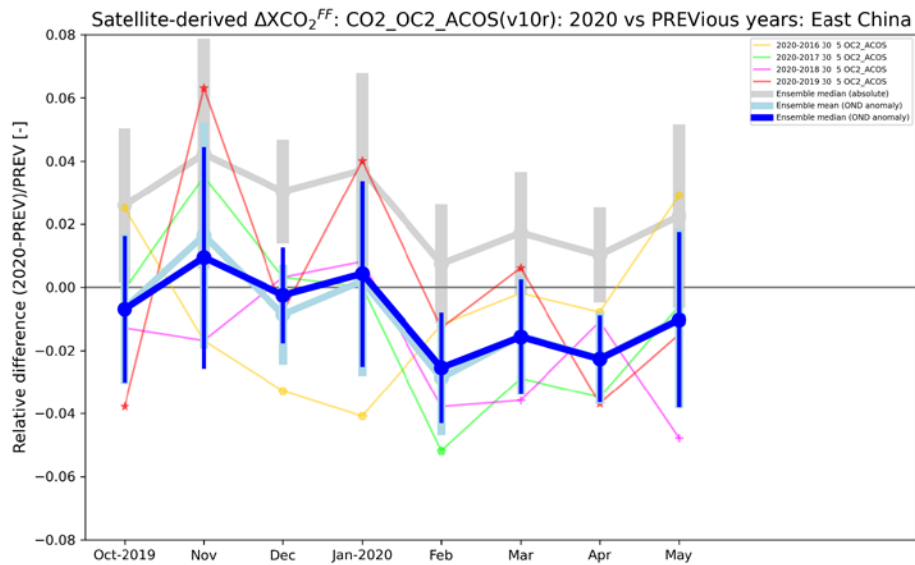


Figure 7: DAM analysis of the OCO-2 ACOS version 10r XCO₂ product (CO₂_OC2_ACOS) for the region East China from January 2015 to May 2020. **Top:(a)** The thin grey line shows the daily DAM XCO₂ anomalies, i.e., daily ΔXCO_2^{DAM} . The red dots are the corresponding monthly values. **Middle: Monthly ΔXCO_2^{FF} .** The red dots (and lines) refer to the time period, which are also shown in (b) for different October – May periods. (c) As (b) but for CO₂^{FF(DAM)}, i.e., for the estimated East China monthly FF emissions (see main text). The data for October 2019 – May 2020, the blue dots to period October 2018 – May (10,2019, the green dots to period October 2017 – May 2018, etc. (see annotation). Bottom panel: the same as the middle panel but for relative differences of the monthly values: Blue dots: relative difference of the values of the red dots shown in the middle panel (ending May_5,2020) and the blue dots are shown in the middle panel (ending May-2019) denoted in the annotation as “(2020-2019)/2019”. Also shown are

150 ~~the relative red~~ (see annotation for other periods). (d) Relative $\text{CO}_2^{\text{FF(DAM)}}$ differences for different periods. In blue, for example, ~~the differences for 2020 and 2018 (green), 2020 and 2017 (orange) and 2020 and 2016 (pink); correspond to the period 10.2019-5.2020 (shown in red in panel (c)) minus 10.2018-5.2019 (shown in blue in (c)).~~ (e) As (d) but after the October to December mean value (“OND anomalies”). The following parameters have been used to generate this figure: Minimum number of observations/day: 30, minimum number of days/month: 5.



Michael.Buchwitz@iup.physik.uni-bremen.de, 17-August-2020

Figure 8: Product CO₂-OC2-ACOS ΔXCO₂^{FF}-differences as shown in the bottom panel of Fig. 7 but including the corresponding median, mean and scatter. The relative differences as shown in the bottom panel of Fig. 7 are shown here via small symbols with thin connecting lines (using different colours for different years, see annotation) and with an offset subtracted, which corresponds to the October-to-December (OND) 2019 mean value, i.e., the data are shown here as anomaly relative to OND 2019 (“OND anomaly²³”). The corresponding median and standard deviation is shown in royal blue (the corresponding mean and standard deviation is shown in light blue). The median of the original data (no offset subtracted) is shown as thick grey dots and lines, i.e., the offset is the difference between the royal blue and the grey lines.

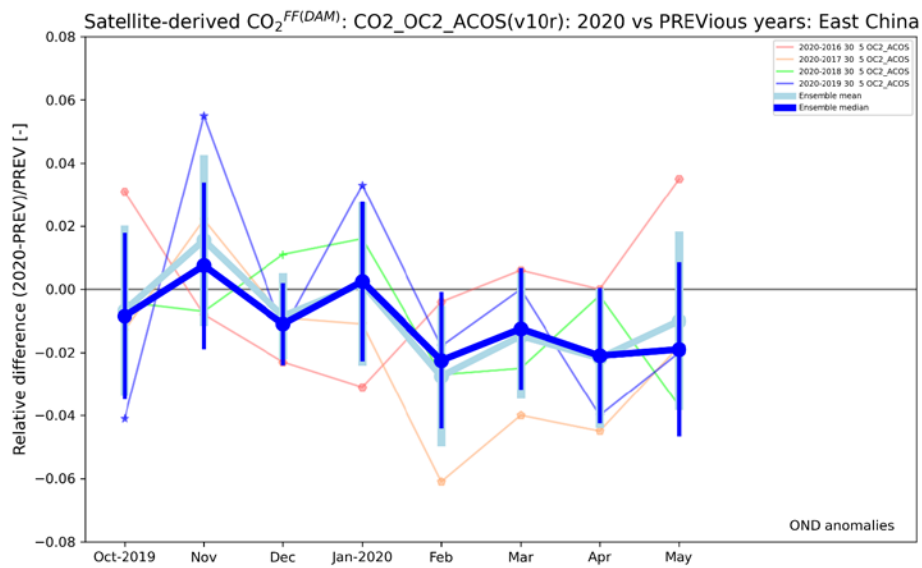
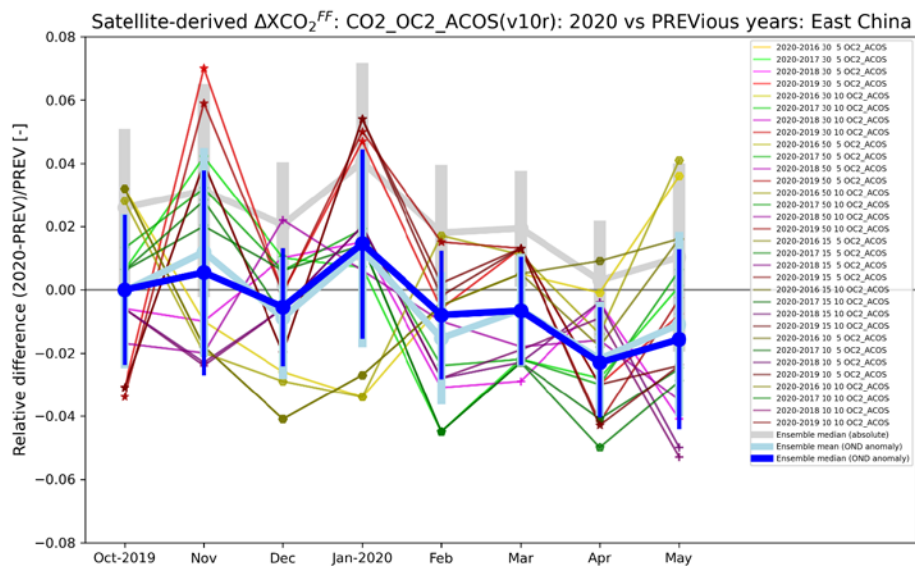
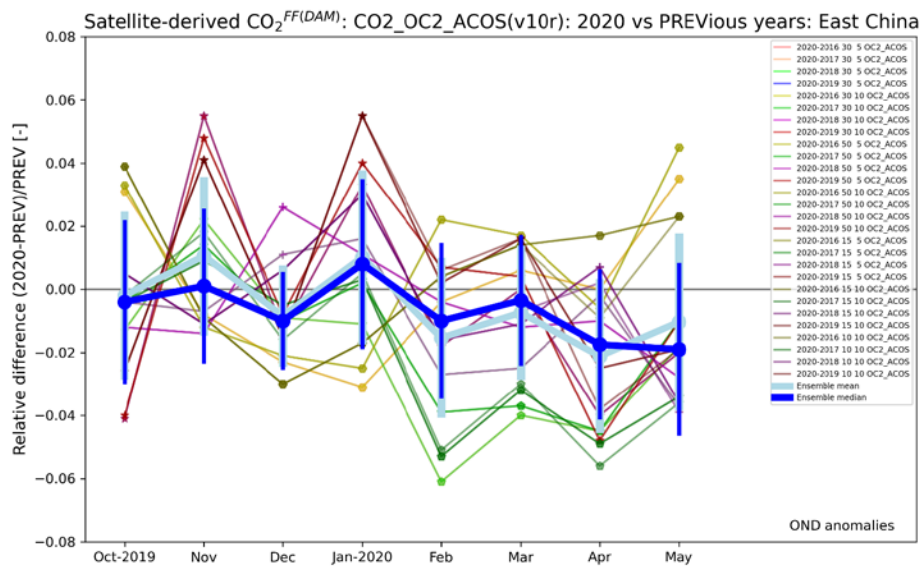


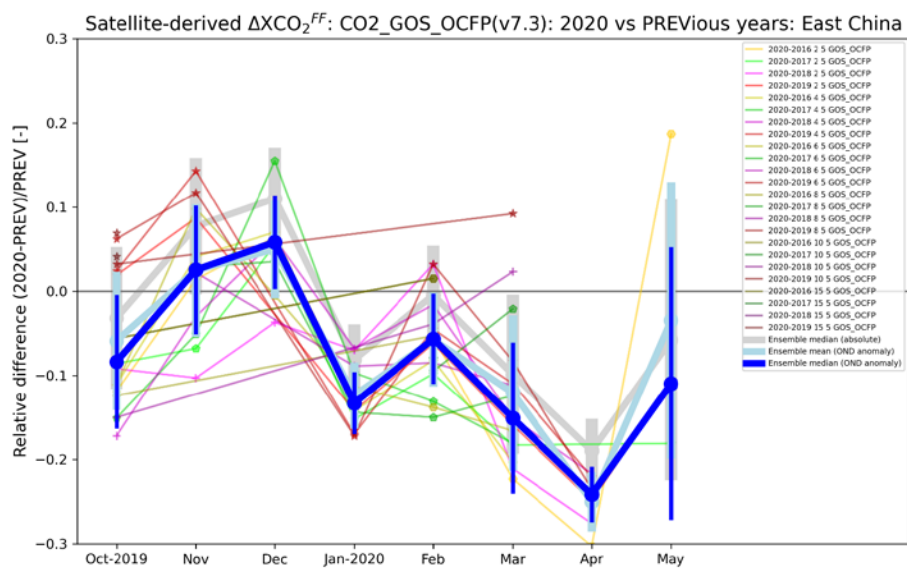
Figure 8: Ensemble members $\text{CO}_2^{\text{FF(DAM)}}$ OND anomalies derived from satellite product CO2_OC2_ACOS . The thin lines and small symbols show the same data also shown in the bottom panel of Fig. 7. The thick dots and lines show the corresponding ensemble median, mean and scatter. The following parameters have been used to generate this figure (see also annotation): Minimum number of observations/day: 30; minimum number of days/month: 5.





Michael Buchwitz@iup.physik.uni-bremen.de, 29-January-2021

Figure 9: The same as Fig. 8 but with additional combinations of minimum number of observations/day (30 as in Fig. 8 and in addition: 50, 15 and 10) and minimum number of days/month (5 as in Fig. 8 and in addition 10) (see annotation).



Michael.Buchwitz@iup.physik.uni-bremen.de, 14-August-2020

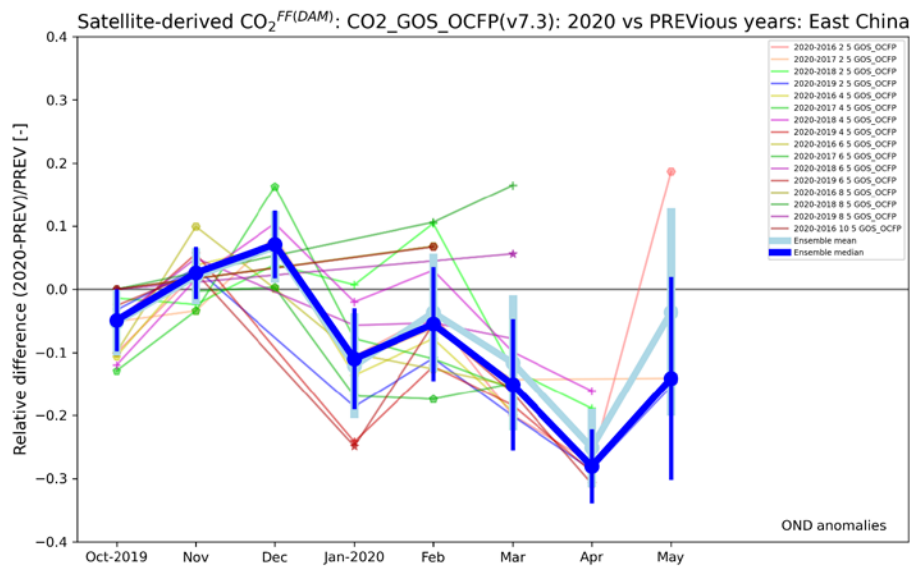
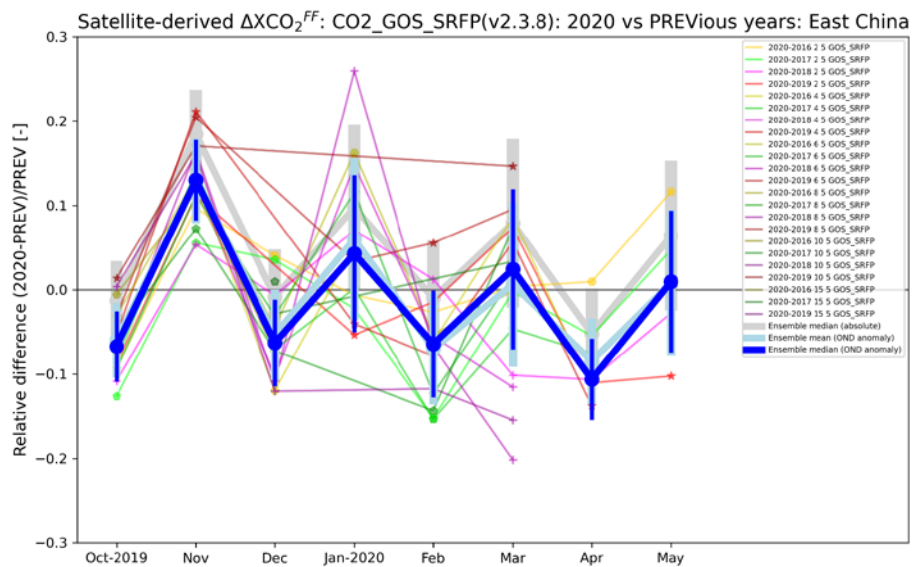
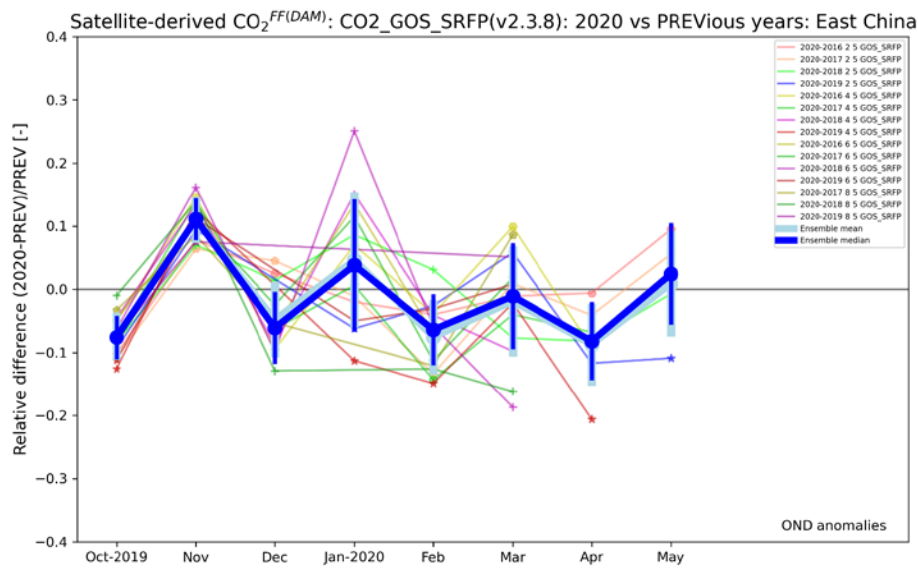


Figure 10: The same as Figs. 9 but for the product $\text{CO}_2\text{_GOS_OCFP}$. Results are shown for several values of the required minimum number of observations/day: 2, 4, 6, 8, 10 and 15. The required minimum number of days/month is 5.

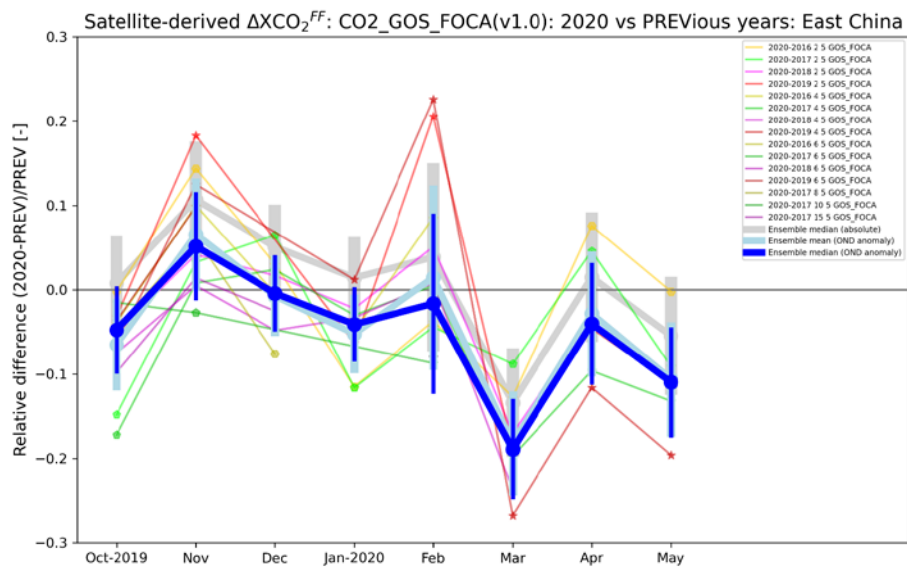


Michael Buchwitz@iup.physik.uni-bremen.de, 26-August-2020



Michael Buchwitz@iup.physik.uni-bremen.de, 29-January-2021

1195 Figure 11: The same as Fig. 10 but for the product CO2_GOS_SRFP .



Michael Buchwitz@iup.physik.uni-bremen.de, 27-August-2020

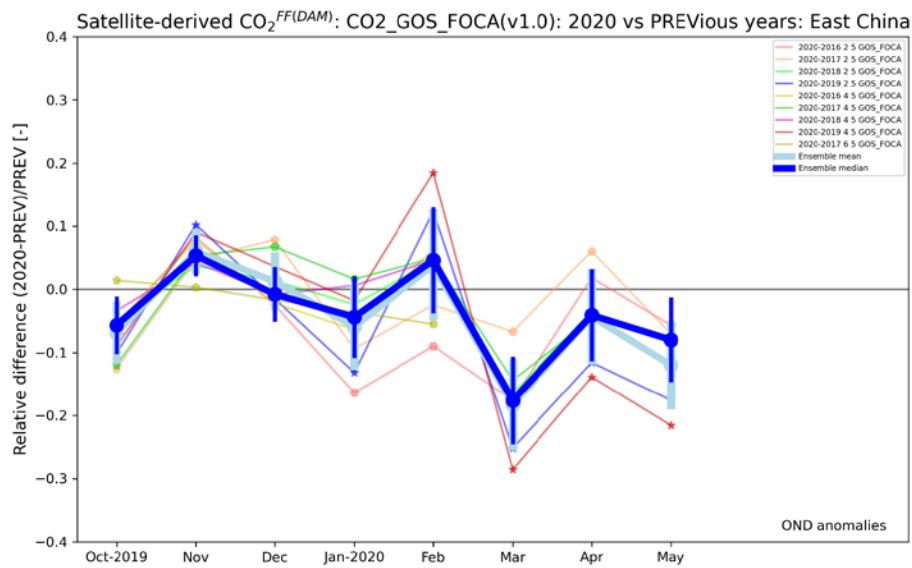
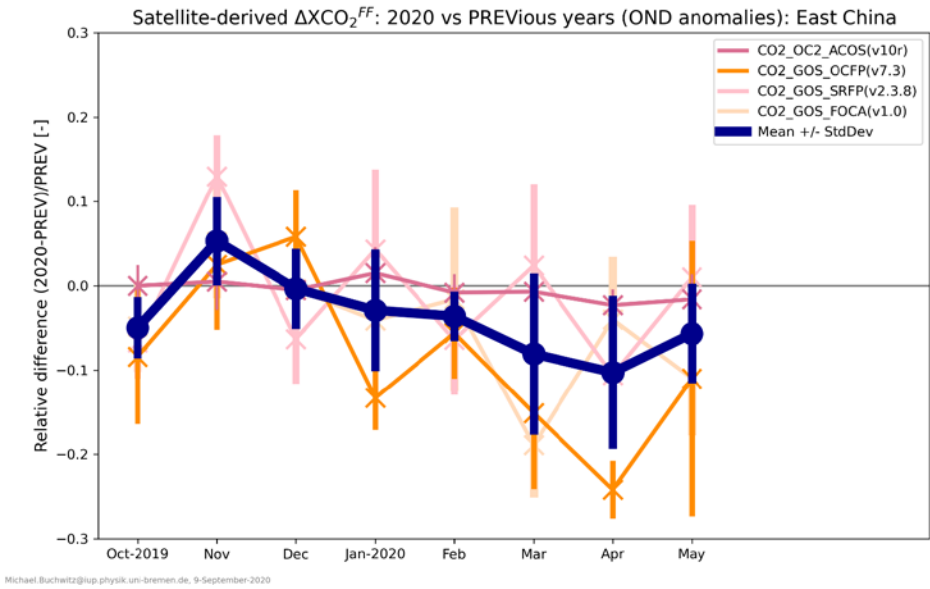
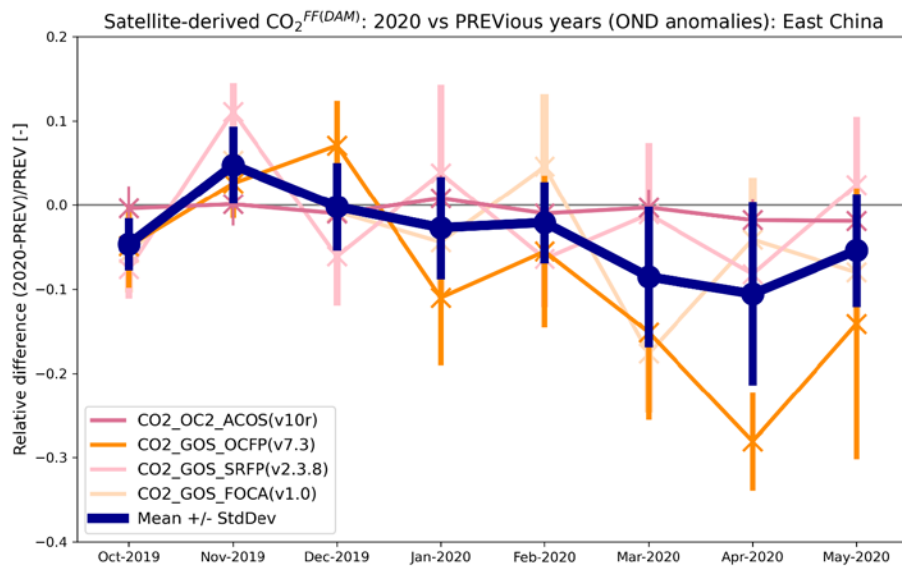


Figure 12: The same as Fig. 10 but for the product CO2_GOS_FOCA.





Michael Buchwitz@iup.physik.uni-bremen.de, 1-February-2021

Figure 13: Overview of the ensemble-based $\text{AXCO}_2^{\text{FFCO}_2^{\text{FFDAM}}}$ results for January-May 2020 relative to October-December 2019 and previous years (also shown in Figs. 9 – 12) via reddish colours for each of the four analysed satellite XCO_2 data products (see Tab. 1). The corresponding ensemble mean value and its uncertainty is shown in dark blue. The uncertainty has been computed as standard deviation of the ensemble members. The corresponding numerical values of the ensemble members are listed in Tab. 4.

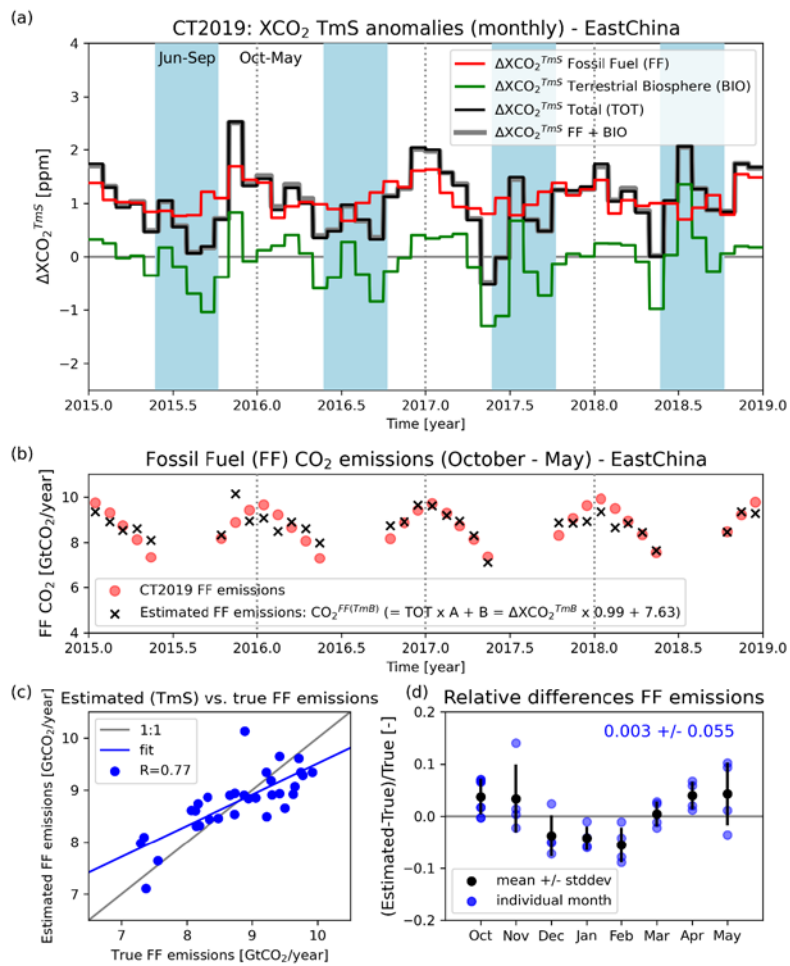


Figure A1: The same as Fig. 2 but using the Target minus Surrounding (TmS) method.

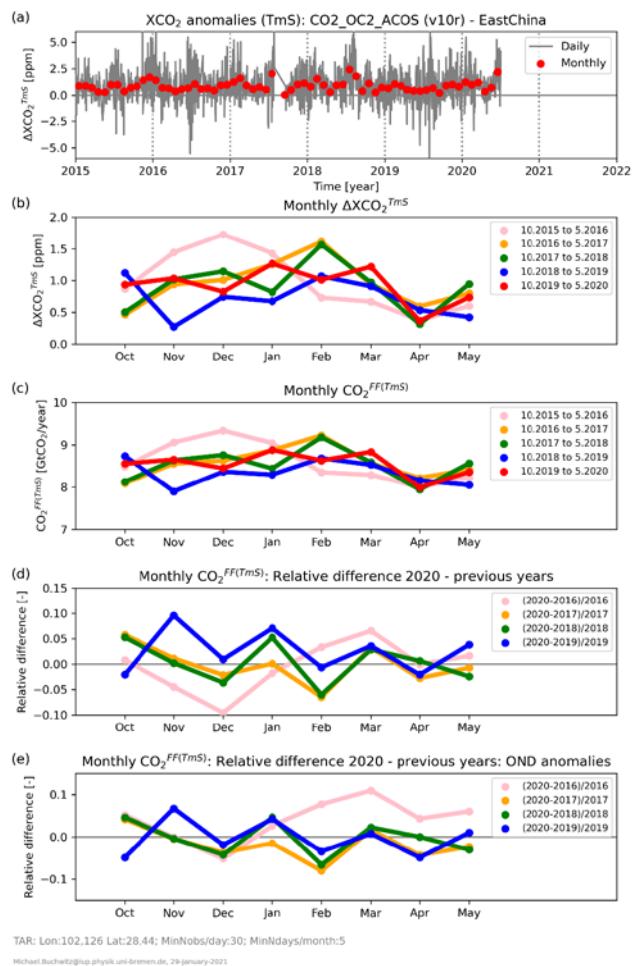
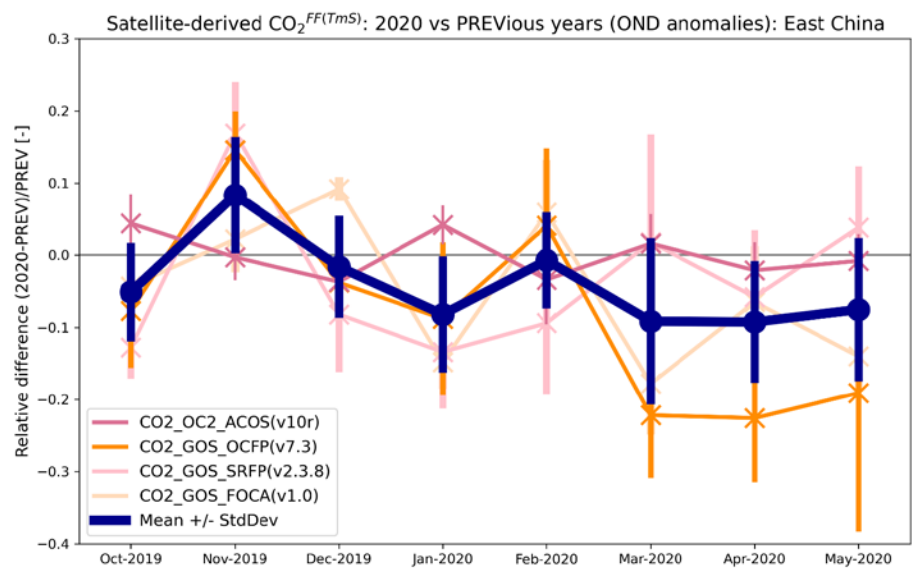


Figure A2: The same as Fig. 7 but using the TmS method.

1225



Michael Buchwitz@iup.physik.uni-bremen.de, 1. February 2021

Figure A3: The same as Fig. 13 but using the TmS method.

1230